

Revisiting Neutrino Masses In Clockwork Models

Aadarsh Singh^{1,*}

¹*Indian Institute Of Science, CV Raman Rd, Bengaluru, Karnataka 560012, India*

(Dated: July 19, 2024)

In this paper, we have looked at various variants of the clockwork model and studied their impact on the neutrino masses. Some of the generalizations such as generalized CW and next-to-nearest neighbour interaction CW have already been explored by a few authors. In this study, we studied non-local CW for the fermionic case and found that non-local models relax the $|q| > 1$ constraint to produce localization of the zero mode. We also made a comparison among them and have shown that for some parameter ranges, non-local variants of CW are more efficient than ordinary CW in generating the hierarchy required for the ν mass scale. Finally, phenomenological constraints from $BR(\mu \rightarrow e\gamma)$ FCNC process and Higgs decay width have been imposed on the parameter space in non-local and both-sided clockwork models. We have listed benchmark points which are surviving current experimental bounds from MEG and are within the reach of the upcoming MEG-II experiment.

* aadarshsingh@iisc.ac.in

I. INTRODUCTION

Neutrino masses are one of the most intriguing problems in flavour physics. To generate eV scale masses from natural weak scales of 100 GeV, it would require a suppression of $O(10^{12})$ in mass scale which seems unnatural. Several mechanisms have been proposed over the last 45 years starting with the seesaw mechanism and its variants Type II and Type III, etc. and then radiative mechanisms including the Zee and Scotogenic model etc. effective operators which generate neutrino masses [1],[2],[3],[4],[5],[6], [7],[8]. While the most natural mechanism of neutrino masses consists of Majorana neutrinos, in recent times enough attention has also been given to Dirac neutrino models. To explain the hierarchical nature of flavour parameters like masses & mixing angles, people have suggested localization of wavefunction approach such as in extra dimension models [9],[10],[11],[12],[13],[14]. This wavefunction localization approach can be used to explain neutrino mass hierarchy as is done by several authors [15],[16],[17],[18],[19],[20]. Equivalently localization can occur in theory space in deconstruction picture. That leads to the production of a highly suppressed Yukawa coupling and hence can be used to explain the required $O(10^{12})$ magnitude suppression in mass scale. Few authors have tried to explain clockwork structures using warped extra dimensions too that lead to a connection between clockwork and linear dilaton theory [21],[18],[15]. This clockwork approach has also been used by various authors to explain inflation, gravity, flavour mixing, axion, dark matter and various other shortcomings of SM [22],[17],[23],[24],[25],[26],[27].

In this paper, firstly we have explored variants of clockwork models where the links in the theory space have been modified but the underlying suppression mechanism is kept intact. Some authors have already explored the generalized clockwork [28] and next-to-nearest neighbour clockwork [29] and the both-sided clockwork scenario is similar to latticized extra dimension so results for these scenarios are known in the literature. We have modified these scenarios and applied them to fermions and found analytical expressions for the 0-mode eigenvector which for non-local theory spaces has a combinatorial factor in it. Since the factorial grows much faster than the exponential, the 0-mode localization can be bigger than the exponential localization such as in randomness-assisted models [30]. However, for the models discussed here, the 0-mode components exhibit combinatorial rather than factorial dependence and, as a consequence, are unable to surpass the exponential. Also, we have described a fine-cancellation mechanism rather than the suppression mechanism to generate a hierarchical scale from the weak scale. This fine cancellation mechanism when implemented for neutrino mass generation, is capable of generating eV scale from TeV scale with natural orders for parameters. The couplings

generated between SM and BSM fields are not tiny so these models are phenomenologically easily testable compared to suppression-based models. The cancellation mechanism is implemented in theory space that resembles the discretized extra dimension model.

The phenomenological signatures for models have been explored using the Flavor-changing neutral current (FCNC) of charged SM leptons. The SM with non-zero neutrino masses contribution for the branching ratio of $\mu \rightarrow e\gamma$ decay comes from one loop corrections and is significantly small $\approx O(10^{-55})$. However, the introduction of these BSM-heavy neutral leptons drastically increases these BR numbers to within the grasp of current experimental bounds. The current most stringent bound for this decay comes from MEG with bound at $BR < 4.2 \times O(10^{-13})$ [31] and can be used to restrict the parameter space of these models. We have given the benchmark points for these models producing the observed neutrino mass that survive the current MEG bounds but are within the reach of upcoming MEG-2 bounds $BR < 6 \times O(10^{-14})$ [32].

The paper begins by studying the clockwork variant models in section 2 & 3. In section 2, the model studied is both-sided clockwork (BCW) and it is shown that the suppression produced in this case is a few orders of magnitude stronger than CW for certain values of parameters. In section 3, non-local clockwork models are studied. The analytical expression of 0-mode for a few cases is given and it is shown that they contain a combinatorial term which for a certain range of parameters gives much bigger suppression than CW. In section 4, we revisited the neutrinos in Large extra dimension (LED) models from a dimensional deconstruction (DD) perspective. We have shown that localization of wavefunctions in this scenario is not a required condition to produce small masses and hence generated neutrino mass scales from TeV scales using only natural parameters. Finally, in section 5 a detailed analysis of BSM effects on FCNC BR is given and some comments about phenomenology in colliders and the contribution of these BSM fields to Higgs mass & width have been made.

Throughout the paper we consider the following neutrino mass and mixing values [33], [34]:

Hierarchy	$\Delta m_{21}^2 (eV^2)$	$\Delta m_{32}^2 (eV^2)$
Normal Hierarchy	$7.39^{+0.21}_{-0.20} \times 10^{-5}$	$2.449^{+0.032}_{-0.030} \times 10^{-3}$
Inverted Hierarchy	$7.39^{+0.21}_{-0.20} \times 10^{-5}$	$-2.509^{+0.032}_{-0.032} \times 10^{-3}$

TABLE I: Neutrino mass-squared differences for Normal and Inverted Hierarchy cases at 1σ range.

Hierarchy	$\theta_{12} (^{\circ})$	$\theta_{23} (^{\circ})$	$\theta_{13} (^{\circ})$
Normal Hierarchy	$33.82^{+0.78}_{-0.76}$	$48.3^{+1.2}_{-1.9}$	$8.61^{+0.13}_{-0.13}$
Inverted Hierarchy	$33.82^{+0.78}_{-0.76}$	$48.6^{+1.1}_{-1.5}$	$8.65^{+0.13}_{-0.12}$

TABLE II: Values of θ_{12} , θ_{23} , and θ_{13} for Normal and Inverted Hierarchy cases at 1σ range.

II. LOCAL CLOCKWORK MODELS - MASS MODEL

The clockwork (CW) models use mechanisms based on suppression by heavy scales to obtain hierarchically small couplings, leading to mass scales that are much smaller than the fundamental parameters of the model. The full Lagrangian is described as

$$\mathcal{L} = \mathcal{L}_{SM} + \mathcal{L}_{NP} + \mathcal{L}_{int}$$

with \mathcal{L}_{SM} representing the lagrangian for the standard model given by

$$\mathcal{L}_{SM} = \mathcal{L}_{Gauge} + \mathcal{L}_{Fermion} + \mathcal{L}_{Higgs} + \mathcal{L}_{Yukawa}$$

\mathcal{L}_{NP} represents the physics of new fields and \mathcal{L}_{int} is the interaction lagrangian between SM fields and new fields. For the new physics lagrangian, we will consider chiral fermionic fields with only Dirac couplings.

$$\mathcal{L}_{NP} = \mathcal{L}_{kin} - \sum_{i,j=1}^n \bar{L}_i \mathcal{H}_{i,j} R_j + h.c. \quad (1)$$

with $\mathcal{H}_{i,j}$ being the Hamiltonian representing the connection between different fields. L_i and R_i represent the clockwork gear fields.

The Hamiltonian and new physics Lagrangian for the generalized CW are given below [28] :-

$$\mathcal{H}_{i,j} = m_i \delta_{i,j} + m_i q_i \delta_{i+1,j} \quad (2)$$

$$\mathcal{L}_{NP} = \mathcal{L}_{kin} - \sum_i^n m_i \bar{L}_i R_i - \sum_i^n m_i q_i \bar{L}_i R_{i+1} + h.c. \quad (3)$$

Corresponding to $\lambda_0 = 0$ eigenvalue, the eigenvector for the GCW is given by

$$\Lambda_0 = \{(-1)^n q_n q_{n-1} \dots q_1, (-1)^{n-1} q_n q_{n-1} \dots q_2, \dots, (-1)^1 q_n, 1\},$$

$$\tilde{\Lambda}_0 = \mathcal{N}_0 \Lambda_0$$

with \mathcal{N}_0 as the normalizing factor and $\tilde{\Lambda}_0$ is the normalized 0-mode. Hence for $q_i > 1$, there will be suppression in the components of 0-mode eigenvector as it will be localized on a certain site. This case along with its various phenomenology has been explored by [28]. The uniform CW (UCW) model is a limiting scenario of generalized CW with $q_i = q \ \forall \ i$ is studied in [15],[16].

A. Both sided Clockwork

This scenario is an extension of CW Hamiltonian where fermions of both chiralities are connected to each other for neighbouring matter fields. The Hamiltonian is diagrammatically represented in Fig. 1 and is written as

$$\mathcal{H}_{i,j} = m_i \delta_{i,j} + m_i q_i \delta_{i+1,j} + q'_i m_i \delta_{i,j+1} \quad (4)$$

$$\mathcal{L}_{NP} = \mathcal{L}_{kin} - \sum_i^n m_i \bar{L}_i R_i - \sum_i^n m_i q_i \bar{L}_i R_{i+1} - \sum_i^{n-1} m_i q'_i \bar{L}_{i+1} R_i + h.c. \quad (5)$$

with $i \in \{1, 2, \dots, n\}$ and $j \in \{1, 2, \dots, n+1\}$ and L_i and R_i being the clockwork gear fields. This Hamiltonian looks similar to the deconstruction scenario but qualitatively it is quite different. In the deconstruction scenario, 0-mode was not always produced, certain relations among fundamental parameters have to be satisfied and also there were constraints on the size of the lattice for 0-mode to exist but in both-sided CW all fundamental parameters can be independent of each other along with the arbitrary number of lattice sites, 0-mode is always produced as seen in the theorem in Appendix-A. Thus this gives us much more freedom from the constraints of fundamental parameters to work with. The matrix for fermionic mass in this model in $\{\bar{L}_1, \bar{L}_2, \dots, \bar{L}_n\}$ and $\{R_1, R_2, \dots, R_{n+1}\}$ basis is given by

$$M_{BCW} = \begin{bmatrix} m_1 & q_1 m_1 & 0 & 0 & \dots & 0 & 0 & 0 \\ q'_1 m_1 & m_2 & q_2 m_2 & 0 & \dots & 0 & 0 & 0 \\ 0 & q'_2 m_2 & m_3 & q_3 m_3 & \dots & 0 & 0 & 0 \\ \vdots & \vdots & \vdots & \ddots & \ddots & \vdots & \vdots & \vdots \\ 0 & 0 & 0 & \dots & \dots & q'_{n-1} m_{n-1} & m_n & q_n m_n \end{bmatrix}_{n \times n+1}$$

Once again, the right-handed fermions will have a 0-mode as per theorem implies. The null basis for right-fermionic field matrix $M_{CW}^\dagger M_{CW}$ is same as the null basis of M_{CW} as

$$M_{CW}^\dagger M_{CW} \Lambda_0 = M_{CW}^\dagger (M_{CW} \Lambda_0) = M_{CW}^\dagger (\vec{0}) = \vec{0}$$

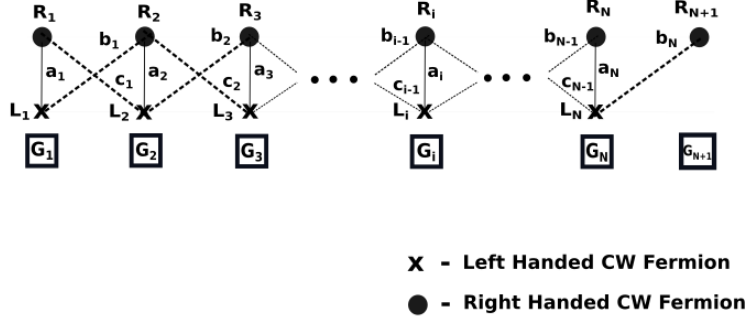


FIG. 1: CW with both-sided interactions. In CW notations, $a_i = m_i$, $b_i = m_i q_i$ and $c_i = m_i q'_i$.

In the uniform limit, the 0-mode eigenvector behaves as

$$\begin{pmatrix} 1 & q & 0 & 0 & \dots & 0 & 0 & 0 \\ q' & 1 & q & 0 & \dots & 0 & 0 & 0 \\ 0 & q' & 1 & q & \dots & 0 & 0 & 0 \\ \vdots & \vdots & \vdots & \ddots & \ddots & \vdots & \vdots & \vdots \\ 0 & 0 & 0 & \dots & \dots & q' & 1 & q \end{pmatrix} \begin{pmatrix} v_1 \\ v_2 \\ v_3 \\ \vdots \\ v_{n+1} \end{pmatrix} = \vec{0}$$

This gives the following recurrence relation for the 0-mode component

$$q'v_{i-1} + v_i + qv_{i+1} = 0, \quad i \in \{2, 3, \dots, n\}$$

with a boundary condition $v_1 = -qv_2$. Solving the recurrence relation with boundary condition we get the k^{th} component value as

$$v_k = c 2^{-k} \left(\left(-\frac{\sqrt{1-4qq'}+1}{q} \right)^k - \left(\frac{\sqrt{1-4qq'}-1}{q} \right)^k \right)$$

where c is some arbitrary constant. It is fixed by imposing the normalization condition on the null vector $\sum_{i=1}^{n+1} v_i^* v_i = 1$.

$$c = \frac{1}{\sqrt{\sum_{i=1}^{n+1} \left\{ 2^{-k} \left(\left(-\frac{\sqrt{1-4qq'}+1}{q} \right)^k - \left(\frac{\sqrt{1-4qq'}-1}{q} \right)^k \right) \right\}^2}}$$

The eigenvalues for $n = 2$ case are given by

$$\lambda_i = \left\{ 0, \frac{m^2}{2} \left(-\sqrt{\left(-(q'_1)^2 - q_1^2 - q_2^2 - 2 \right)^2 - 4 \left(q_1^2 (q'_1)^2 - 2q_1 q'_1 + q_1^2 q_2^2 + q_2^2 + 1 \right)} + (q'_1)^2 + q_1^2 + q_2^2 + 2 \right), \frac{m^2}{2} \left(\sqrt{\left(-(q'_1)^2 - q_1^2 - q_2^2 - 2 \right)^2 - 4 \left(q_1^2 (q'_1)^2 - 2q_1 q'_1 + q_1^2 q_2^2 + q_2^2 + 1 \right)} + (q'_1)^2 + q_1^2 + q_2^2 + 2 \right) \right\} \quad (6)$$

and unnormalized 0-mode eigenvector is given by

$$\Lambda_0 = \left\{ -\frac{q_1 q_2}{q_1 q'_1 - 1}, \frac{q_2}{q_1 q'_1 - 1}, 1 \right\} \quad (7)$$

Hence as $q'_1 \rightarrow \frac{1}{q_1}$, the 0-mode becomes more and more localized. In uniform limit, $q_i = q$ and $q'_i = q'$ $\forall i$, the eigenvalues and 0-mode eigenvector is

$$\lambda_i = \left\{ 0, -\frac{m^2}{2} \sqrt{4(q' + q)^2 + q'^4} + 1 + \frac{q'^2}{2} + q^2, \frac{m^2}{2} \sqrt{4(q' + q)^2 + q'^4} + 1 + \frac{q'^2}{2} + q^2 \right\}$$

$$\Lambda_0 = \left\{ -\frac{q^2}{q'q - 1}, \frac{q}{q'q - 1}, 1 \right\}$$

the first component of 0-mode will be greater than that in the normal CW model for $|q'q - 1| < 1$. As $q' \rightarrow \frac{1}{q}$, first two components $\rightarrow \infty$ hence 0-mode localization on last site $\rightarrow 0$.

$$(q|q') \in \mathbb{R}, \left(q' < 0 \wedge \frac{2}{q'} < q < 0 \right) \vee \left(q' > 0 \wedge 0 < q < \frac{2}{q'} \right) \quad (8)$$

for these sets of values, the double-sided CW model will produce greater suppression than ordinary CW. For $n = 2$, $q = -3$, CW produces 10^{-1} order suppression but for these set of values with $q' = -0.33$, this model produces 10^{-3} order of suppression which is $O(2)$ magnitude bigger suppression than CW. Similarly, the 0-mode eigenvector for $n = 3$ in the uniform limit can be found

$$\Lambda_0 = \left\{ \frac{q^3}{2qq' - 1}, -\frac{q^2}{2qq' - 1}, -\frac{q(qq' - 1)}{2qq' - 1}, 1 \right\} \quad (9)$$

again the first component of 0-mode will be greater than that in the normal CW model for $|2q'q - 1| < 1$. In this model apart from CW localization of q^n in the numerator of the first component of 0-mode, there is a denominator too which depends on the extra parameter introduced by coupling left-handed fermions of i^{th} group to the right-handed fermions of $(i - 1)^{th}$ group. The suppression of coupling produced will be more than CW in this scenario for the following set of parameters

$$(q|q') \in \mathbb{R}, \left(q' < 0 \wedge \frac{1}{q'} < q < 0 \right) \vee \left(q' > 0 \wedge 0 < q < \frac{1}{q'} \right)$$

For $n = 3$ and $q = -2$, CW produces 10^{-1} order suppression whereas this model with $q' = -0.24$, produces 10^{-3} order suppression, 2 orders smaller than ordinary CW.

To compare with CW, we took $n = 40$ gears with $q = -2$ to produce eV mass from the TeV scale but here it can be done with $n = 20$ for $q = -2$ and $q' = -0.15$. To get large localization, we took both q and q' to be of the same sign. For opposite signs, as can be seen from eq.(9), the denominator would not be that small and so localization will not be that large. This model will work better than CW for parameter values of $q' \in [-0.539, 0]$, there are three more intervals of smaller length but choosing q' from those intervals will convert the natural hierarchy problem into the fine-tuning problem.

Now to study the effect of SM neutrino coupling with CW fermions perturbatively, we will consider the interaction term in Lagrangian of the same form as in GCW.

$$\mathcal{L}_{int} = -Y\tilde{H}\bar{L}_L R_{n+1} + \text{h.c.} \quad (10)$$

The Dirac mass matrix in the basis $\{\bar{\nu}, \bar{L}_n, \bar{L}_{n-1}, \dots, \bar{L}_1\}$ and $\{R_{n+1}, R_n, R_{n-1}, \dots, R_1\}$ for $Y = 0$ is given by

$$\tilde{M} = m \begin{bmatrix} 0 & 0 & 0 & 0 & \dots & 0 \\ q & 1 & q' & 0 & \dots & 0 \\ 0 & q & 1 & q' & \dots & 0 \\ \vdots & \vdots & \vdots & \ddots & \ddots & \vdots \\ 0 & 0 & 0 & \dots & q & 1 \end{bmatrix}_{(n+1) \times (n+1)}$$

The masses for right-handed CW fermions will be again given by $m\sqrt{\tilde{\lambda}_i}$, with $\tilde{\lambda}_i$ denoting the eigenvalues of the matrix $\tilde{M}^\dagger \tilde{M}/m^2$.

$$\widetilde{M}^\dagger \widetilde{M} = m^2 \begin{bmatrix} q^2 & q & qq' & 0 & \dots & 0 \\ q & 1+q^2 & q+q' & qq' & \dots & 0 \\ qq' & q+q' & 1+q^2+q'^2 & q+q' & \dots & 0 \\ \vdots & \vdots & \vdots & \ddots & \ddots & \vdots \\ 0 & 0 & 0 & \dots & q+q' & 1+q'^2 \end{bmatrix}_{(n+1) \times (n+1)}$$

For non-zero coupling Y , the eigenstates and eigenvalues change depending on the value of Y . Consider p to be the perturbative coupling strength then the Dirac mass matrix \tilde{M} becomes

$$M = m \begin{bmatrix} p & 0 & 0 & 0 & \dots & 0 \\ q & 1 & q' & 0 & \dots & 0 \\ 0 & q & 1 & q' & \dots & 0 \\ \vdots & \vdots & \vdots & \ddots & \ddots & \vdots \\ 0 & 0 & 0 & \dots & q & 1 \end{bmatrix}_{(n+1) \times (n+1)}$$

The right-handed fermions have masses $m\sqrt{\lambda_i}$ with λ_i being the eigenvalues of the following mass matrix:-

$$\frac{M^\dagger M}{m^2} = \begin{bmatrix} p^2 + q^2 & q & qq' & 0 & \dots & 0 \\ q & 1 + q^2 & q + q' & qq' & \dots & 0 \\ qq' & q + q' & 1 + q^2 + q'^2 & q + q' & \dots & 0 \\ \vdots & \vdots & \vdots & \ddots & \ddots & \vdots \\ 0 & 0 & 0 & \dots & q + q' & 1 + q'^2 \end{bmatrix}_{(n+1) \times (n+1)}$$

Again we can write this matrix as the sum of the Dirac matrix without Yukawa neutrino coupling and a perturbation matrix.

$$M^\dagger M = \tilde{M}^\dagger \tilde{M} + \delta M^2$$

with perturbation matrix given by

$$\delta M^2 = m^2 \begin{bmatrix} p^2 & \mathbf{0}_{1 \times n} \\ \mathbf{0}_{n \times 1} & \mathbf{0}_{n \times n} \end{bmatrix}_{(n+1) \times (n+1)}$$

As the perturbation matrix in CW fermions basis is again independent of neighbouring CW coupling strength parameters and depends on SM field coupling strength and the mass scale, the leading-order corrections to the eigenvalues are proportional to p .

$$\delta \lambda_i = \left\langle \Lambda^{(i)} \left| \frac{\delta M^2}{m^2} \right| \Lambda^{(i)} \right\rangle = p^2 f(q, q') = O(p^2)$$

again Λ_i denotes eigenvectors of the unperturbed matrix for BCW (both-sided clockwork) case eq.(5) and $f(q, q')$ denotes function f coming from the dependence of eigenvector Λ'_i 's components on variables q and q' . Once again the leading order corrections are of the second order with respect to p . In this

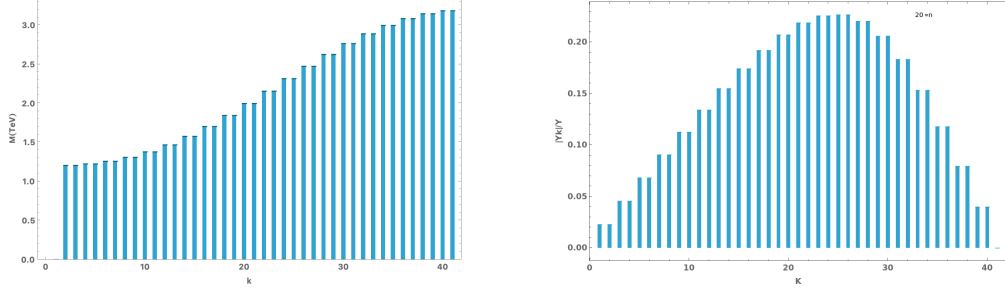


FIG. 2: The left plot shows the mass distribution and the right plot shows the coupling strength for the general clockwork scenario with $n = 20$ clockwork fermions.

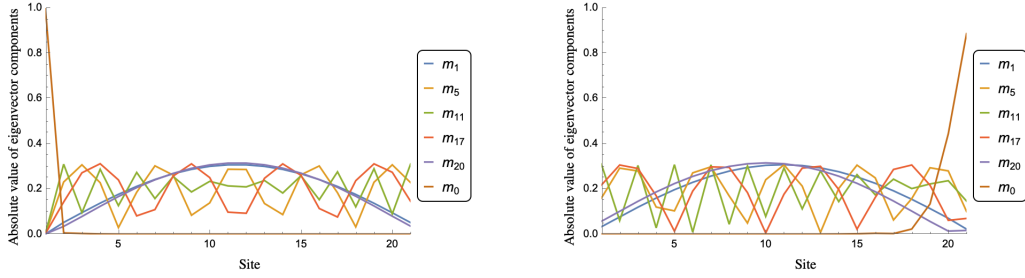


FIG. 3: The left plot shows the absolute value of left-handed mass eigenvectors in terms of CW fields and the right plot for right-handed mass eigenbasis with $y = 0.1$.

scenario too, the perturbative eigenvector analysis in the appendix of [28] holds true up to the order of p .

The KK mass spectrum for Clockwork gears and their coupling strength with SM neutrino is shown in Fig. 2. For this scenario $n = 20$ gears are considered with $m_i = 1$ TeV, $q_i = -3$ and $q'_i = -0.2$. Fig. 3 demonstrates the localization of different eigenvectors in CW fields on different sites. The Yukawa coupling strength to SM neutrino y is considered to be 0.1.

Hierarchy	n	q	q'	Yukawa Couplings
Normal	50	-5	-5/3	$\{y_1, y_2, y_3\} = \{0.1, 0.113, 0.32\}$
Inverted	50	-5	-5/3	$\{y_1, y_2, y_3\} = \{0.3155, 0.32, 0.1\}$

TABLE III: BP points for the model with $q_i = q, q'_i = q' \quad \forall i \in \{1, 2, \dots, n\}$

producing neutrino mass in agreement with experimental data and avoiding phenomenological constraints.

III. NON-LOCAL CLOCKWORK MODELS

A. NNN CW

In non-local CW theory space, matter fields corresponding to groups which are not adjacent in the theory space/moose diagram also have link fields connecting them. These connections are formulated in the model by modifying the underlying Hamiltonian in the Lagrangian of the model. The Hamiltonian for NNN-CW (next-to-nearest neighbour clockwork) is given by

$$\mathcal{H}_{i,j} = m_i \delta_{i,j} + q_i^{(1)} m_i \delta_{i+1,j} + q_i^{(2)} \delta_{i+2,j} \quad (11)$$

$$\mathcal{L}_{NP} = \mathcal{L}_{kin} - \sum_i^n m_i \bar{L}_i R_i - \sum_i^n m_i q_i^{(1)} \bar{L}_i R_{i+1} - \sum_i^{n-1} m_i q_i^{(2)} \bar{L}_i R_{i+2} + h.c. \quad (12)$$

with $i \in \{1, 2, \dots, n\}$ and $j \in \{1, 2, \dots, n+1\}$. In this model too, the mass matrix for right-handed

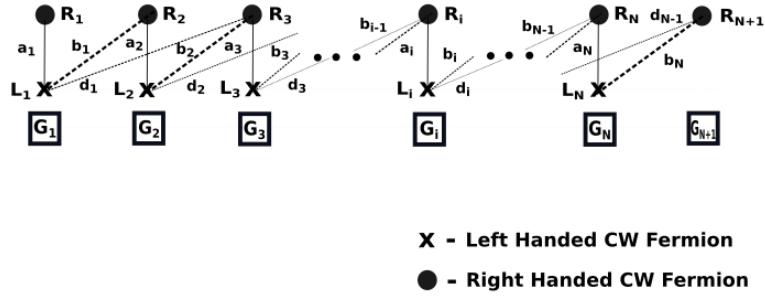


FIG. 4: CW with NNN (Next to Nearest Neighbour) interactions. In CW notations, $a_i = m_i$, $b_i = m_i q_i^{(1)}$ and $d_i = m_i q_i^{(2)}$.

CW fermions will have a 0 mode as per the theorem. The matrix for the above Hamiltonian 11 in $\{\bar{L}_1, \bar{L}_2, \dots, \bar{L}_n\}$ and $\{R_1, R_2, \dots, R_{n+1}\}$ basis is given by

$$M_{CW} = \begin{bmatrix} m_1 & m_1 q_1^{(1)} & m_1 q_1^{(2)} & 0 & \dots & 0 \\ 0 & m_2 & m_2 q_2^{(1)} & m_2 q_2^{(2)} & \dots & 0 \\ 0 & 0 & m_3 & m_3 q_3^{(1)} & \dots & 0 \\ \vdots & \vdots & \vdots & \ddots & \ddots & \vdots \\ 0 & 0 & \dots & m_{n-1} & m_{n-1} q_{n-1}^{(1)} & m_{n-1} q_{n-1}^{(2)} \\ 0 & 0 & 0 & \dots & m_n & m_n q_n^{(1)} \end{bmatrix}_{n \times n+1}$$

The K^{th} component for null space basis of NNN CW in the uniform limit case, $m_i = m$, $q_i^{(1)} = q$ and $q_i^{(2)} = q' \forall i$ is given by

$$\Lambda_0^K = \sum_{\{k_i, k_j\}} \frac{(k_i + k_j)!}{k_i! k_j!} \frac{(-mq')^{k_i} (-mq)^{k_j}}{m^{k_i + k_j}} \quad (13)$$

$$\text{with} \quad 2k_i + k_j = n + 1 - K \quad (14)$$

$$\Lambda_0 = \{\Lambda_0^1, \Lambda_0^2, \dots, \Lambda_0^{n+1}\}$$

k_i and $k_j \in \mathbb{N}_0 = \{0, 1, 2, 3, 4, \dots\}$. The normalized 0-mode $\tilde{\Lambda}_0$ is given by $\mathcal{N}_0 \Lambda_0$, with \mathcal{N}_0 representing the normalizing factor. Using $\tilde{\Lambda}_0^\dagger \tilde{\Lambda}_0 = 1$, we get

$$\mathcal{N}_0 = \frac{1}{\sqrt{\sum_{i=1}^{n+1} \Lambda_0^{i*} \Lambda_0^i}}$$

The 0-mode eigenvector for $n = 2$ case is

$$\Lambda_0 = \left\{ -\frac{m_2 m_1 q_1^{(2)} - m_1 q_1^{(1)} m_2 q_2^{(2)}}{m_1 m_2}, -\frac{m_2 q_2^{(1)}}{m_2}, 1 \right\} \quad (15)$$

in the uniform limit, $m_i = m$, $m_i q_i^{(1)} = mq$ and $m_i q_i^{(2)} = q' \forall i$, it will reduce to

$$\Lambda_0 = \{-(q' - q^2), -q, 1\}$$

it will produce bigger suppression than CW for

$$(q|q') \in \mathbb{R}, (q < 0 \wedge (q' \leq 0 \vee q' \geq 2q^2)) \vee q = 0 \vee (0 < q \wedge (q' \leq 0 \vee q' \geq 2q^2))$$

Now for $n = 3$ in the limiting case, the 0-mode eigenvector is

$$\{-(q^3 - 2qq'), -(q' - q^2), -q, 1\} \quad (16)$$

with conditions

$$(q|q') \in \mathbb{R}, (q < 0 \wedge (q' < 0 \vee q' > q^2 - q^3)) \vee (0 < q \wedge (q' < 0 \vee q' > q^3 + q^2))$$

it produces greater suppression than CW.

To compare with CW, we took $n = 40$ gears with $m = 1$ TeV, $q = -2$ to produce $O(1)$ eV mass from the TeV scale, here it can be done with $n = 25$ for $q = -2$ and $q' = -3$. One will notice that we took $-ve$ values for coupling parameters q_i , this is necessary to get bigger components in 0-mode, for $+ve$ values of q_i , the components cancel within themselves as can be seen in eq.(16) and hence does

not give large localization. Apart from faster localization, the NNN CW model relaxes the condition of $q > 1$ for localization to take place. This model achieves localization even for $q = 1$ due to extra combinatorics factors in the components of 0-mode. Again to study the effect of SM neutrino coupling with NNN CW fermions perturbatively, we will consider the interaction term in Lagrangian of the same form as before eq.(10).

$$\mathcal{L}_{int} = -Y\tilde{H}\bar{L}_L R_{n+1} + \text{h.c.} \quad (17)$$

The Dirac mass matrix in the basis $\{\bar{\nu}, \bar{L}_n, \bar{L}_{n-1}, \dots, \bar{L}_1\}$ and $\{R_{n+1}, R_n, R_{n-1}, \dots, R_1\}$ for $Y = 0$ is given by

$$\tilde{M} = m \begin{bmatrix} 0 & 0 & 0 & 0 & \dots & 0 \\ q & 1 & 0 & 0 & \dots & 0 \\ q' & q & 1 & 0 & \dots & 0 \\ 0 & q' & q & 1 & \dots & 0 \\ \vdots & \vdots & \vdots & \ddots & \ddots & \vdots \\ 0 & 0 & 0 & \dots & q & 1 \end{bmatrix}_{(n+1) \times (n+1)}$$

The masses for right-handed CW fermions will be again given by $m\sqrt{\tilde{\lambda}_i}$, with $\tilde{\lambda}_i$ denoting the eigenvalues of the matrix $\tilde{M}^\dagger \tilde{M}/m^2$.

$$\tilde{M}^\dagger \tilde{M} = m^2 \begin{bmatrix} q^2 + q'^2 & q + qq' & q' & 0 & \dots & 0 & 0 \\ q + qq' & 1 + q^2 + q'^2 & q + qq' & q' & \dots & 0 & 0 \\ q' & q + qq' & 1 + q^2 + q'^2 & q + qq' & \dots & 0 & 0 \\ \vdots & \vdots & \vdots & \ddots & \ddots & \vdots & \vdots \\ 0 & 0 & \dots & q' & q + qq' & 1 + q^2 & q \\ 0 & 0 & \dots & 0 & q' & q & 1 \end{bmatrix}_{(n+1) \times (n+1)}$$

For non-zero coupling Y , the eigenstates and eigenvalues change depending on the value of Y . Consider p to be the perturbative coupling strength then the Dirac mass matrix \tilde{M} becomes

$$M = m \begin{bmatrix} p & 0 & 0 & 0 & \dots & 0 \\ q & 1 & 0 & 0 & \dots & 0 \\ q' & q & 1 & 0 & \dots & 0 \\ 0 & q' & q & 1 & \dots & 0 \\ \vdots & \vdots & \vdots & \ddots & \ddots & \vdots \\ 0 & 0 & 0 & \dots & q & 1 \end{bmatrix}_{(n+1) \times (n+1)}$$

The right-handed fermions have masses $m\sqrt{\lambda_i}$ with λ_i being the eigenvalues of the following mass matrix:-

$$\frac{M^\dagger M}{m^2} = \begin{bmatrix} p^2 + q^2 + q'^2 & q + qq' & q' & 0 & \dots & 0 & 0 \\ q + qq' & 1 + q^2 + q'^2 & q + qq' & q' & \dots & 0 & 0 \\ q' & q + qq' & 1 + q^2 + q'^2 & q + qq' & \dots & 0 & 0 \\ \vdots & \vdots & \vdots & \ddots & \ddots & \vdots & \vdots \\ 0 & 0 & \dots & q' & q + qq' & 1 + q^2 & q \\ 0 & 0 & \dots & 0 & q' & q & 1 \end{bmatrix}_{(n+1) \times (n+1)}$$

Again we can write this matrix as the sum of the Dirac matrix with 0 neutrino coupling and a perturbation matrix.

$$M^\dagger M = \tilde{M}^\dagger \tilde{M} + \delta M^2$$

with perturbation matrix given by

$$\delta M^2 = m^2 \begin{bmatrix} p^2 & \mathbf{0}_{1 \times n} \\ \mathbf{0}_{n \times 1} & \mathbf{0}_{n \times n} \end{bmatrix}_{(n+1) \times (n+1)}$$

As the perturbation matrix in CW fermions basis is again independent of neighbouring CW coupling strength parameters and depends on SM field coupling strength, the leading-order corrections to the eigenvalues are proportional to p .

$$\delta \lambda_i = \left\langle \Lambda^{(i)} \left| \frac{\delta M^2}{m^2} \right| \Lambda^{(i)} \right\rangle = p^2 f(q, q') = O(p^2)$$

again Λ_i denotes eigenvectors of unperturbed matrix for next-to-nearest neighbour clockwork (NNN-CW) case and $f(q, q')$ denotes function f coming from dependence of eigenvector Λ_i 's components on variables q and q' . Once again the leading order corrections are of the second order with respect to p . In this scenario too, the perturbative eigenvector analysis in the appendix of [28] holds true up to the order of p .

The KK mass spectrum for Clockwork gears and their coupling strength with SM neutrino is shown in Fig. 5. For this scenario $n = 20$ gears are considered with $m_i = 1$ TeV, $q_i = -2$ and $q'_i = -3$. Fig. 6 demonstrates the localization of different eigenvectors in CW fields on different sites. The Yukawa coupling strength to SM neutrino y is considered to be 0.1.

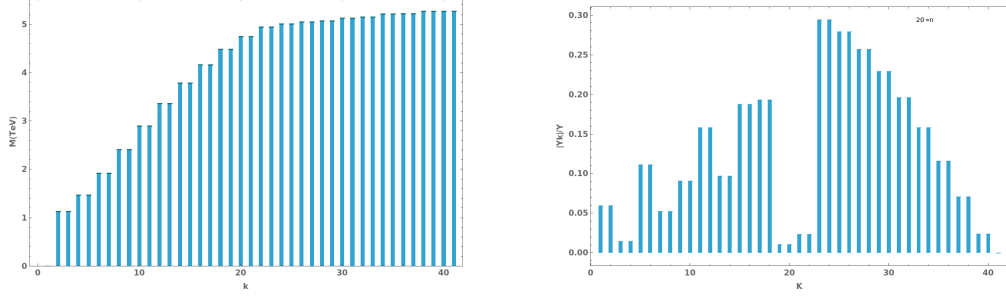


FIG. 5: The Left plot shows the mass distribution and the right plot shows the coupling strength for the NNN clockwork scenario with $n = 20$ clockwork fermions.

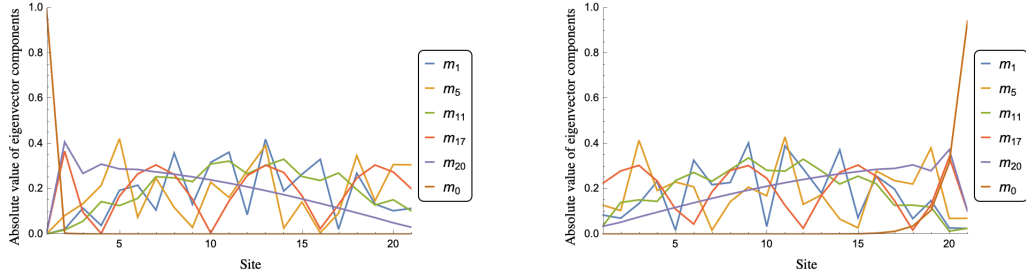


FIG. 6: The left plot shows the absolute value of left-handed mass eigenvectors in terms of CW fields and the right plot for right-handed mass eigenbasis with $y = 0.1$.

Hierarchy	n	q	q'	Yukawa Couplings
Normal	15	-5	-5	$\{y_1, y_2, y_3\} = \{0.1, 0.101, 0.13\}$
Inverted	15	-5	-5	$\{y_1, y_2, y_3\} = \{0.1, 0.101, 0.06\}$

TABLE IV: BP points for the model with $q_i = q, q'_i = q' \quad \forall i \in \{1, 2, \dots, n\}$

producing neutrino mass in agreement with experimental data.

B. Completely Non-local CW

In this further extension scenario, we will consider fully non-local theory spaces i.e., theory spaces where the matter fields of each group are connected via link fields to the matter fields of every other group. The underlying Hamiltonian is still considered as rectangular, implying that the number of left chiral fermions is not equal to the number of right chiral fermions. The CW nature of theory space is retained. The theory space is diagrammatically shown in Fig. 7. Hamiltonian for this extension can

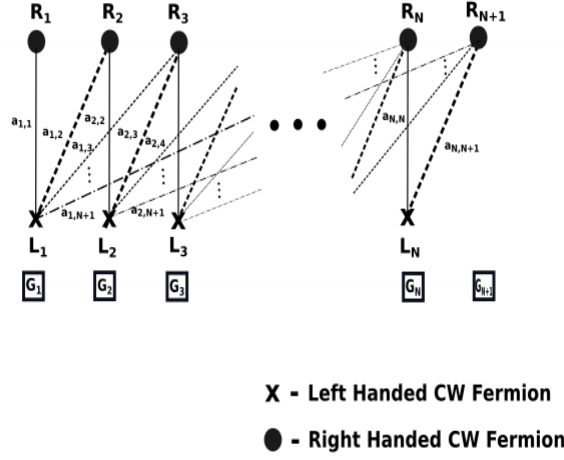


FIG. 7: CW with all neighbouring interactions. In CW notations, $a_{i,i} = m_i$, $a_{i,i+1} = m_i q_i^{(1)}$, $a_{i,i+2} = m_i q_i^{(2)}$, \dots , $a_{i,i+n} = m_i q_i^{(n)}$.

be written as

$$\mathcal{H}_{i,j} = \sum_{k=1}^{n+1} a_{i,k} \delta_{i,j-k+1} \quad (18)$$

with $i \in \{1, 2, \dots, n\}$ and $j \in \{1, 2, \dots, n+1\}$. Using the CW notation to write the new physics Lagrangian, one gets

$$\begin{aligned} \mathcal{L}_{NP} &= \mathcal{L}_{kin} - \sum_{i=1}^n m_i \bar{L}_i R_i - \sum_{i=1}^n m_i q_i^{(1)} \bar{L}_i R_{i+1} - \sum_{i=1}^{n-1} m_i q_i^{(2)} \bar{L}_i R_{i+2} - \sum_{i=1}^{n-2} m_i q_i^{(3)} \bar{L}_i R_{i+3} \\ &\quad - \sum_{i=1}^{n-3} m_i q_i^{(4)} \bar{L}_i R_{i+4} + \dots - \sum_{i=1}^{n-(n-1)} m_i q_i^{(n)} \bar{L}_i R_{i+n} + h.c. \\ &= \mathcal{L}_{kin} - \sum_{i=1}^n m_i \bar{L}_i R_i - \sum_{k=1}^n \sum_{i=1}^{n-k+1} m_i q_i^{(k)} \bar{L}_i R_{i+k} + h.c. \end{aligned} \quad (19)$$

In this model, the mass matrix for right-handed CW fermions will also have a 0 mode as per the theorem since the Hamiltonian is rectangular. The matrix for this Hamiltonian in $\{\bar{L}_1, \bar{L}_2, \dots, \bar{L}_n\}$ and

$\{R_1, R_2, \dots, R_{n+1}\}$ basis is given by

$$M_{CW} = \begin{bmatrix} a_{1,1} & a_{1,2} & a_{1,3} & a_{1,4} & \dots & a_{1,n+1} \\ 0 & a_{2,2} & a_{2,3} & a_{2,4} & \dots & a_{2,n+1} \\ 0 & 0 & a_{3,3} & a_{3,4} & \dots & a_{3,n+1} \\ \vdots & \vdots & \vdots & \ddots & \ddots & \vdots \\ 0 & 0 & \dots & a_{n-1,n-1} & a_{n-1,n} & a_{n-1,n+1} \\ 0 & 0 & 0 & \dots & a_{n,n} & a_{n,n+1} \end{bmatrix}_{n \times n+1}$$

In CW notations, $a_{i,i} = m_i$, $a_{i,i+1} = m_i q_i^{(1)}$, $a_{i,i+2} = m_i q_i^{(2)}$, \dots , $a_{i,i+n} = m_i q_i^{(n)}$. The K^{th} component for null space basis of CN-CW (completely non-local clockwork) in the limiting case, $a_{i,i+k} = a_k \forall i$, is given by

$$\Lambda_0^K = \sum_{\{k_1, \dots, k_n\}} \frac{(k_1 + k_2 + \dots + k_n)!}{k_1! \dots k_n!} \frac{(-a_n)^{k_n} \dots (-a_1)^{k_1}}{a_0^{k_1 + k_2 + \dots + k_n}} \quad (20)$$

$$\text{with} \quad nk_n \dots + 2k_2 + k_1 = n + 1 - K \quad (21)$$

$$\Lambda_0 = \{\Lambda_0^1, \Lambda_0^2, \dots, \Lambda_0^{n+1}\}$$

and $k_1, k_2, \dots, k_n \in \mathbb{N}_0 = \{0, 1, 2, 3, 4, \dots\}$. The normalized 0-mode $\tilde{\Lambda}_0$ is given by $\mathcal{N}_0 \Lambda_0$, with \mathcal{N}_0 representing the normalizing factor. Using $\tilde{\Lambda}_0^\dagger \tilde{\Lambda}_0 = 1$, we get

$$\mathcal{N}_0 = \frac{1}{\sqrt{\sum_{i=1}^{n+1} \Lambda_0^{i*} \Lambda_0^i}}$$

To compare with CW, it took $n = 40$ gears with $a = 1$, $q = -2$ to produce $O(1)$ eV mass from the TeV scale, here it can be done with $n = 25$ for $a_0 = 1$, $a_1 = -2$, $a_2 = -3$ and $a_i = -2$, $i \in [3, n]$. However, compared to the NNN CW model, this model does not give orders of extra suppression unless hierarchy in fundamental parameters a_i s are introduced.

Now same as earlier, to study the effect of SM neutrino coupling with CW fermions perturbatively, we will consider the interaction term in Lagrangian of the same form as before eq.(10).

$$\mathcal{L}_{int} = -Y \tilde{H} \bar{L}_L R_{n+1} + \text{h.c.} \quad (22)$$

The Dirac mass matrix in the basis $\{\bar{\nu}, \bar{L}_n, \bar{L}_{n-1}, \dots, \bar{L}_1\}$ and $\{R_{n+1}, R_n, R_{n-1}, \dots, R_1\}$ for $Y = 0$ is given by

$$\tilde{M} = m \begin{bmatrix} 0 & 0 & 0 & 0 & \dots & 0 \\ q & 1 & 0 & 0 & \dots & 0 \\ q & q & 1 & 0 & \dots & 0 \\ q & q & q & 1 & \dots & 0 \\ \vdots & \vdots & \vdots & \ddots & \ddots & \vdots \\ q & q & q & \dots & q & 1 \end{bmatrix}_{(n+1) \times (n+1)}$$

for simplicity, the case with the same value for all couplings is considered. The masses for right-handed CW fermions will be again given by $m\sqrt{\tilde{\lambda}_i}$, with $\tilde{\lambda}_i$ denoting the eigenvalues of the matrix $\tilde{M}^\dagger \tilde{M}/m^2$.

$$\tilde{M}^\dagger \tilde{M} = m^2 \begin{bmatrix} nq^2 & q + (n-1)q^2 & q + (n-2)q^2 & q + (n-3)q^2 & \dots & q + q^2 & q \\ q + (n-1)q^2 & 1 + (n-1)q^2 & q + (n-2)q^2 & q + (n-3)q^2 & \dots & q + q^2 & q \\ q + (n-2)q^2 & q + (n-2)q^2 & 1 + (n-2)q^2 & q + (n-3)q^2 & \dots & q + q^2 & q \\ \vdots & \vdots & \vdots & \ddots & \ddots & \vdots & \vdots \\ q + q^2 & q + q^2 & \dots & q + q^2 & q + q^2 & 1 + q^2 & q \\ q & q & \dots & q & q & q & 1 \end{bmatrix}_{(n+1) \times (n+1)}$$

For non-zero coupling Y , the eigenstates and eigenvalues change depending on the value of Y . Consider p to be the perturbative coupling strength then the Dirac mass matrix \tilde{M} becomes

$$M = m \begin{bmatrix} p & 0 & 0 & 0 & \dots & 0 \\ q & 1 & 0 & 0 & \dots & 0 \\ q & q & 1 & 0 & \dots & 0 \\ q & q & q & 1 & \dots & 0 \\ \vdots & \vdots & \vdots & \ddots & \ddots & \vdots \\ q & q & q & \dots & q & 1 \end{bmatrix}_{(n+1) \times (n+1)}$$

The right-handed fermions have masses $m\sqrt{\lambda_i}$ with λ_i being the eigenvalues of the following mass matrix:-

$$\frac{M^\dagger M}{m^2} = \begin{bmatrix} p^2 + nq^2 & q + (n-1)q^2 & q + (n-2)q^2 & q + (n-3)q^2 & \dots & q + q^2 & q \\ q + (n-1)q^2 & 1 + (n-1)q^2 & q + (n-2)q^2 & q + (n-3)q^2 & \dots & q + q^2 & q \\ q + (n-2)q^2 & q + (n-2)q^2 & 1 + (n-2)q^2 & q + (n-3)q^2 & \dots & q + q^2 & q \\ \vdots & \vdots & \vdots & \ddots & \ddots & \vdots & \vdots \\ q + q^2 & q + q^2 & \dots & q + q^2 & q + q^2 & 1 + q^2 & q \\ q & q & \dots & q & q & q & 1 \end{bmatrix}_{(n+1) \times (n+1)}$$

Again as in previous cases we can write this matrix as the sum of the Dirac matrix with 0 neutrino coupling and a perturbation matrix.

$$M^\dagger M = \tilde{M}^\dagger \tilde{M} + \delta M^2$$

with perturbation matrix given by

$$\delta M^2 = m^2 \begin{bmatrix} p^2 & \mathbf{0}_{1 \times n} \\ \mathbf{0}_{n \times 1} & \mathbf{0}_{n \times n} \end{bmatrix}_{(n+1) \times (n+1)}$$

The perturbation matrix is independent of the CW coupling strength parameters the same as in earlier variants of CW. And it depends on the Standard Model (SM) field coupling strength. As a result, the leading-order corrections to the eigenvalues of the matrix are proportional to the SM field coupling strength parameter, p .

$$\delta \lambda_i = \left\langle \Lambda^{(i)} \left| \frac{\delta M^2}{m^2} \right| \Lambda^{(i)} \right\rangle = p^2 f(q) = O(p^2)$$

Λ_i denotes eigenvectors of the unperturbed matrix for the CN-CW case. In a general scenario, $f(q^{(1)}, q^{(2)}, q^{(3)}, \dots, q^{(n)})$ will be a function depending on $q^{(i)}$ coupling strength. Once again the leading order corrections are of the second order with respect to p .

The KK mass spectrum for Clockwork gears and their coupling strength with SM neutrino is shown in Fig. 8. For this scenario $n = 20$ gears are considered with $m_i = 1$ TeV, $q_i^{(j)} = -2 \forall i, j$. Fig. 9 demonstrates the localization of different eigenvectors in CW fields on different sites. The Yukawa coupling strength to SM neutrino y is considered to be 0.1. As is evident from the BP of CN-CW the difference in hierarchy produced in this model is not much from the NNN-CW model.

Apart from retaining the clockwork nature of left-right chiral fields in non-local extensions, we can

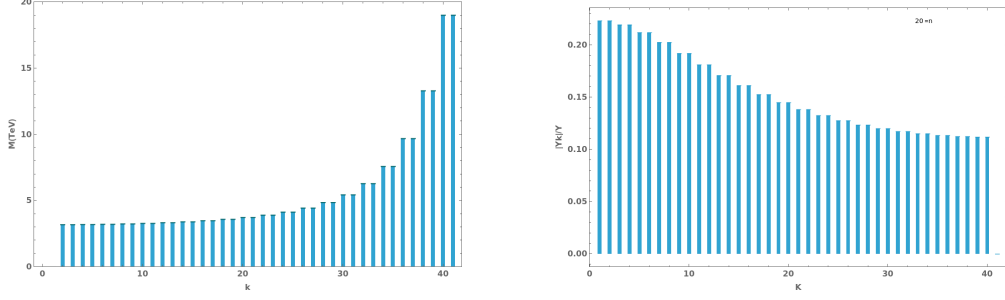


FIG. 8: The left plot shows the mass distribution and the right plot shows the coupling strength for the completely non-local clockwork scenario with $n = 20$ clockwork fermions.

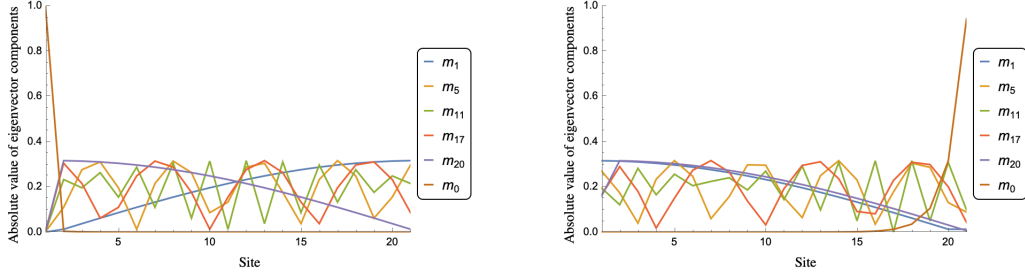


FIG. 9: The left plot shows the absolute value of left-handed mass eigenvectors in terms of CW fields and the right plot for right-handed mass eigenbasis with $y = 0.1$.

Hierarchy	n	q	Yukawa Couplings
Normal	15	-5	$\{y_1, y_2, y_3\} = \{0.1, 0.102, 0.155\}$
Inverted	15	-5	$\{y_1, y_2, y_3\} = \{0.1386, 0.14, 0.08\}$

TABLE V: BP points for the model with $q_i^j = q \ \forall \ i, j$ producing neutrino mass in agreement with experimental data.

consider both-sided non-local CW extensions too. Hamiltonian for this scenario is given by [35]

$$(\mathcal{H}_{\text{long-range}})_{j,k} = a_j \delta_{j,k} + \frac{b}{r^{|j-k|}} (1 - \delta_{j,k}), \quad (23)$$

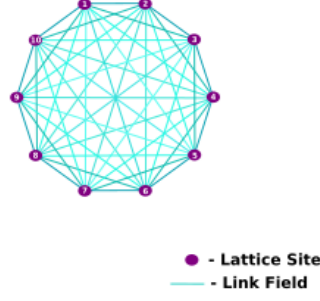


FIG. 10: Completely Non-local interaction for $n = 9$ with both ways interaction. The distance between the two sites is not parallel to their coupling strength.

The Hamiltonian considered is long-range hopping strength decaying Hamiltonian. Dirac mass matrix for this Hamiltonian in $\{\bar{L}_1, \bar{L}_2, \dots, \bar{L}_n\}$ and $\{R_1, R_2, \dots, R_{n+1}\}$ basis is given by

$$M_{\text{long-range}} = \begin{bmatrix} a_1 & \frac{b}{r} & \frac{b}{r^2} & \frac{b}{r^3} & \dots & \frac{b}{r^n} \\ \frac{b}{r} & a_2 & \frac{b}{r} & \frac{b}{r^2} & \dots & \frac{b}{r^{n-1}} \\ \frac{b}{r^2} & \frac{b}{r} & a_3 & \frac{b}{r} & \dots & \frac{b}{r^{n-2}} \\ \vdots & \vdots & \vdots & \ddots & \ddots & \vdots \\ \frac{b}{r^{n-2}} & \frac{b}{r^{n-1}} & \dots & a_{n-1} & \frac{b}{r} & \frac{b}{r^2} \\ \frac{b}{r^{n-1}} & \frac{b}{r^{n-2}} & \frac{b}{r^{n-3}} & \dots & a_n & \frac{b}{r} \end{bmatrix}_{n \times (n+1)}$$

For $n = 2$, in the limiting case, right-hand fermionic eigenvalues are

$$\lambda_i = \left\{ 0, \frac{-b\sqrt{16a^2r^6 + 16abr^4 + b^2r^4 + 2b^2r^2 + b^2} + 2a^2r^4 + 3b^2r^2 + b^2}{2r^4}, \right. \\ \left. \frac{b\sqrt{16a^2r^6 + 16abr^4 + b^2r^4 + 2b^2r^2 + b^2} + 2a^2r^4 + 3b^2r^2 + b^2}{2r^4} \right\}$$

with 0-mode eigenvector given by

$$\Lambda_0 = \left\{ -\frac{ab - b^2}{a^2r^2 - b^2}, -\frac{abr^2 - b^2}{r(a^2r^2 - b^2)}, 1 \right\} \quad (24)$$

Hence as $b \rightarrow ar$, the suppression of 0-mode on the last site increases. Now for $n = 3$, the 0-mode eigenvector has components given by

$$\Lambda_0 = \left\{ -\frac{r(a^2b - 2ab^2 + b^3)}{a^3r^4 - 2ab^2r^2 - ab^2 + 2b^3}, -\frac{ab - b^2}{a^2r^2 + ab - 2b^2}, -\frac{a^2br^4 - ab^2r^2 - ab^2 - b^3r^2 + 2b^3}{r(a^3r^4 - 2ab^2r^2 - ab^2 + 2b^3)}, 1 \right\}$$

Under certain values of b , the suppression on a specific site will be sufficient to generate masses that are hierarchically smaller, in a natural manner.

Finally, we can compare the absolute value of the minimum component of the 0-mode produced by different variants of CW models. The result is shown in Fig. 11 also the parameters considered for models are mentioned.

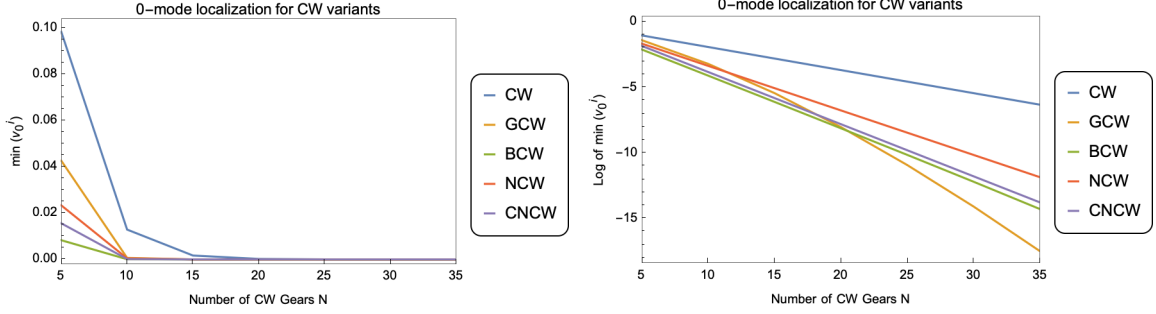


FIG. 11: For these plots, the scenario considered is $q=-1.5$ with $q'=-1/4$ for BCW and $q^i=q$ for NCW and CNCW and $q_i = q - 0.1 \times i$ for GCW. The X-axis represents the number of CW gears considered.

Model	Mass Parameters	Coupling Parameters
CW	$m_i = 1$	$q_i = -1.5$
GCW	$m_i = 1$	$q_i = -1.5 - 0.1 \times i$
BCW	$m_i = 1$	$q = -1.5, q' = -1/4$
NNCW	$m_i = 1$	$q^i = q = -1.5$
CNCW	$m_i = 1$	$q^i = q = -1.5$

TABLE VI: Parameters and descriptions for different Clockwork models with varying number of CW gears.

Even for higher values of q , the trend stays the same i.e., variants of CW are producing bigger localization of 0-mode on a particular site and hence are more efficient to produce hierarchical masses. As shown in Fig. 11, the difference in localization strength increases with the number of gears introduced into the system. This is an expected result, as a greater number of gears leads to a larger combinatorial factor element in the 0-mode component.

IV. FINE CANCELLATION IN DIMENSIONAL DECONSTRUCTION MODELS

Deconstruction models are the latticized extra spatial dimension models [36]. Since, these deconstruction models are the extra dimension models at low energy i.e, the physics produced by these two models at low energy converges, they are termed as dimensional deconstruction (DD) models. The DD models with moose diagrams having only nearest neighbour interactions for a finite number of groups are equivalent to the extra latticized spatial dimension picture for a finite number of sites at low energies. This low-energy extra-dimension physics is reproduced by considering structures among abstract groups at high energies. To set the notation we recap here DD which has been reviewed in several papers [37], [38]. For link fields $\Phi_{i,j}$, the action is given by

$$S_{link} = \int d^4x \left\{ \sum_{i,j=1}^N \left[\text{Tr} \left((D_\mu \Phi_{i,j})^\dagger D^\mu \Phi_{i,j} \right) - \frac{1}{4} F_{i,\mu\nu,a} F^{i,\mu\nu,a} \right] - V(\Phi) \right\} \quad (25)$$

where $a = 1, 2, \dots, m^2 - 1$. The fields are considered to propagate in 4-dimensional spacetime. For SSB to take place, the potential that will produce non-zero *vev* for link fields can be written as

$$V(\Phi) = \sum_{j=1}^N \left[-M'^2 \text{Tr} \left(\Phi_{i,j}^\dagger \Phi_{i,j} \right) + \lambda_1 \text{Tr} \left(\Phi_{i,j}^\dagger \Phi_{i,j} \right)^2 + \lambda_2 \left(\text{Tr} \left(\Phi_{i,j}^\dagger \Phi_{i,j} \right) \right)^2 + M' \left(e^{i\theta} \det(\Phi_{i,j}) + \text{h.c.} \right) \right] \quad (26)$$

For λ_1, λ_2 and $M' > 0$ and $M'^2 < 0$, this potential produces a Mexican hat shape and leads to non-zero *vev* for the link field.

$$S_{matter} = \sum_{i,j=1}^N \int d^4x \left\{ \bar{\psi} (i\gamma^\mu D_\mu) \psi + (\bar{L}_i \Phi_{i,j} R_j + \bar{L}_j \Phi_{j,i} R_i) + \bar{L}_j M R_j + \text{h.c.} \right\} \quad (27)$$

Depending on the *vevs* of link fields various kinds of Hamiltonians and hence theory spaces are produced. If the *vevs* of link fields connecting only the consecutive groups' matter fields are non-zero i.e, $\langle \Phi_{i,j} \rangle \neq 0$ only for $j = i - 1$ and $i + 1$ then one gets a local theory space if it is non-zero for other i and j than one gets non-local theory spaces. The local DD model is equivalent to the ADD model at low energies.

1. One Flavour Scenario

The Hamiltonian in this scenario is the same as the uniform tight-binding model Hamiltonian [39]. The mode localization is not present in this Hamiltonian so the wavefunctions are spread throughout

the sites.

$$\mathcal{L}_{NP} = \mathcal{L}_{kin} - \sum_{i,j=1}^n \overline{L}_i \mathcal{H}_{i,j} R_j + h.c. \quad (28)$$

with

$$\mathcal{H}_{i,j} = \epsilon \delta_{i,j} - t(\delta_{i+1,j} + \delta_{i,j+1}) \quad (29)$$

ϵ & t are the new parameters of the model. This Hamiltonian produces several delocalized modes with eigenmasses and eigenvectors given by (30) & (31)

$$\lambda_k = \epsilon - 2t \cos \frac{k\pi}{n+1}, \quad (30)$$

for $k \in \{1, 2, \dots, n\}$, and the corresponding $\chi_j^{(k)}$, eigenvectors are given by

$$\chi_j^{(k)} = \rho^k \sin \frac{kj\pi}{n+1}, \quad j \in \{1, 2, \dots, n\} \quad (31)$$

where ρ^k is the normalization factor for k^{th} eigenvector.

There is no localization of any kind in this model. Since the Dirac mass matrix is symmetric, the rotation of the left and right modes will be identical as shown in AppendixA. The unitary transformation in diagonalisation will make sure different modes are orthogonal to each other. Since the rotation matrices are unitary, the inner product of different modes will be 0 i.e,

$$\sum_{i=1}^n v_j^i v_k^i = \delta_{j,k}$$

For the SM neutrino interaction to BSM fields with SM Higgs consider the following interaction term in the Lagrangian [9]:¹

$$\mathcal{L}_{int.} = Y \bar{\nu}_L H R_1 + Y \bar{\nu}_R H L_n + h.c.$$

The smallest mass mode for the final mass matrix with weaker couplings Y is given by

$$m_0 \approx v^2 \sum_{i=1}^n \frac{v_1^i v_n^i}{\lambda_i}$$

with v as the expectation value of the Higgs field and v_n^i being the i^{th} component of n^{th} eigenvector.

If $\lambda_i = \lambda \forall i$, then $m_0 \rightarrow 0$ from unitarity condition. For,

$$\begin{aligned} \lambda_i &= \epsilon - 2t \cos \frac{i\pi}{n+1}, \\ \frac{\lambda_i}{\epsilon} &= 1 - \frac{2t}{\epsilon} \cos \frac{i\pi}{n+1}, \end{aligned} \quad (32)$$

¹ This interaction is the same as is considered in [30]. This is similar to localizing left chiral and right chiral neutrinos on opposite branes in RS/ADD, depending on the Higgs profile.

hence for $t \ll \epsilon$, $\frac{\lambda_i}{\epsilon} \rightarrow 1 \forall i$. For this case, the approximate value of m_0 is given as

$$\begin{aligned}
m_0 &\approx v^2 \sum_{i=1}^n \frac{v_1^i v_n^i}{\lambda_i} \\
&= v^2 \sum_{i=1}^n \frac{v_1^i v_n^i}{\epsilon} \frac{\epsilon}{\lambda_i} \\
&= v^2 \frac{1}{\epsilon} \sum_{i=1}^n v_1^i v_n^i (1 - x_i)^{-1} \\
&= \frac{v^2}{\epsilon} \sum_{i=1}^n v_1^i v_n^i + \frac{v^2}{\epsilon} \sum_{i=1}^n v_1^i v_n^i x_i + \dots \\
m_0 &\approx \frac{v^2}{\epsilon} \sum_{i=1}^n v_1^i v_n^i x_i
\end{aligned} \tag{33}$$

where,

$$x_i = \frac{2t}{\epsilon} \cos \frac{i\pi}{n+1}$$

so $x_i \rightarrow 0 \Rightarrow m_0 \rightarrow 0$. This mechanism will work better for matrices whose eigenvalue spectrum has the same range order as in ADD models. For hierarchical spectra as in warped models, this will not work efficiently. As the separation between the magnitude of minimum and maximum eigenvalue increases, this mechanism's effectiveness in producing hierarchical scale decreases.

We find for $\epsilon = 10$, $t = 0.5$ and $n = 8$, we get a small mass of the order 0.1 eV from the TeV scale i.e, $O(0^{12})$ magnitude smaller scale than the fundamental parameter scales of the theory. Fig. 12 shows the mass spectra and eigenvectors for some massive modes for $n = 15$, $t = 0.5$ and $\epsilon = 10$. The figure demonstrates that modes are not localized and mass spectra are close to degenerate. Fig. 13 shows a comparison for the smallest mass scale produced between the DD model, uniform clockwork (UCW) and generalized clockwork (GCW) models. This figure shows that for chosen parameters, the mass scale produced by DD is a few orders of magnitude smaller than both UCW and GCW for various values of sites. Fig. 14 shows the smallest mass scale produced by this model for varying ϵ and t (left) and for varying sites n and t (right). The figure shows that large values of n & ϵ and/or small values of t produce smaller mass scale which is in agreement with the above understanding of the model.

2. Three Flavour Scenario

This can be extended to 3 flavour cases to account for all three SM active neutrino masses. The number of sites for each flavour is taken to be the same with differing flavour neutrinos coupling to

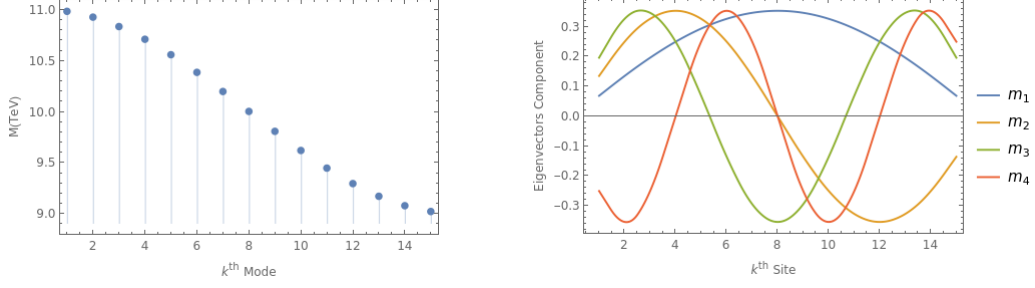


FIG. 12: Figure shows the mass spectrum of modes (left) and eigenvectors for the first four heavy modes (right) for $n = 15$.

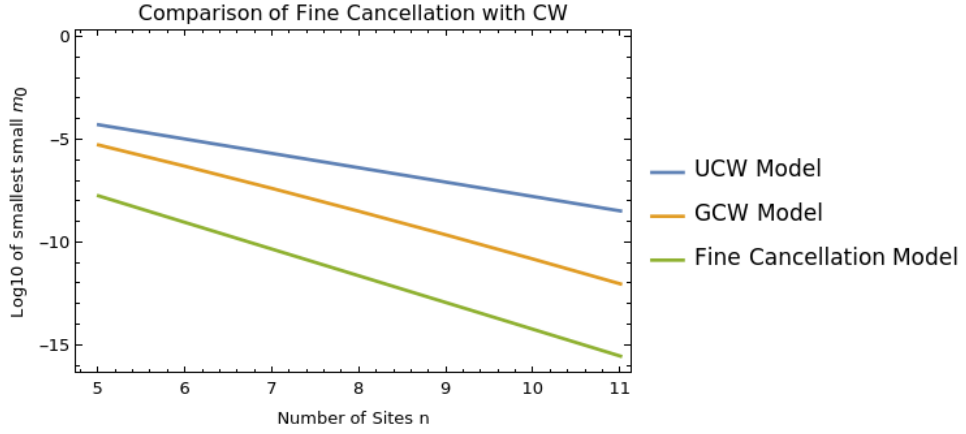


FIG. 13: Figure shows the comparison of the smallest mass-produced by UCW (uniform clockwork) eq.(3) with parameters $m_i = 1$ and $q_i = -5 \forall i \in \{1, n\}$, GCW (generalized clockwork) eq.(3) with parameters $m_i = 1$ and $q_i = -5 - i$, $1 \leq i \leq n$ and Fine Cancellation model with $\epsilon = 10$ and $t = 0.5$ for the varying number of sites n .

Model	Mass Parameters	Coupling Parameters
UCW	$m_i = 1$,	$q_i = -5$
GCW	$m_i = 1$,	$q_i = -5 - i$
Fine Cancellation	$\epsilon = 10$,	$t = 0.5$

TABLE VII: Parameters for comparison of UCW, GCW, and Fine Cancellation models in Fig. 13 with a varying number of sites n .

the BSM fields. These varying couplings will produce different masses for different active neutrinos.

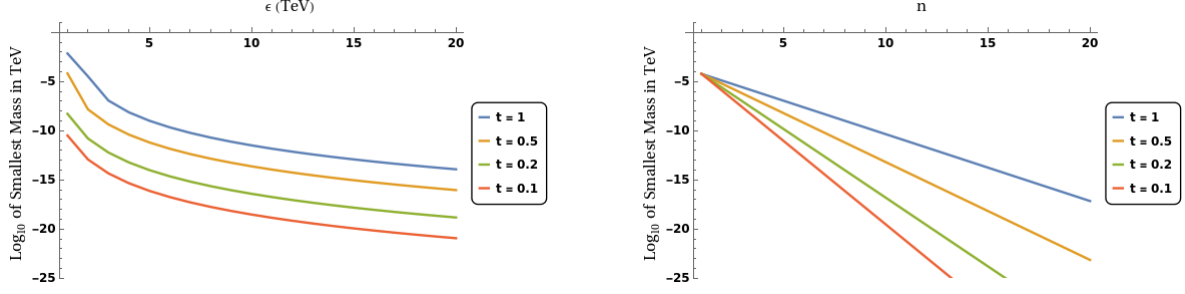


FIG. 14: Figure shows the variation of log of smallest mass scale produced with the model scale parameter ϵ with $n = 8$ (left) and with the number of sites/fields for each flavour (right) with $\epsilon = 5$.

The full 3 flavour Lagrangian for this scenario is given by

$$\mathcal{L}_{NP} = L_{kin} - \sum_{i,j=1}^n \bar{L}_i^{\alpha} \mathcal{H}_{i,j}^{\alpha,\beta} R_j^{\beta} + h.c. \quad (34)$$

$$\mathcal{H}_{i,j}^{\alpha,\beta} = \epsilon_i^{\alpha,\beta} \delta_{i,j} + t^{\alpha,\beta} (\delta_{i+1,j} + \delta_{i,j+1}) \quad (35)$$

with the interaction between different flavours of SM and BSM neutrino fields given by

$$\mathcal{L}_{Int.} = Y_1^{\alpha,\beta} \bar{\nu}_L^{\alpha} H R_1^{\beta} + Y_2^{\alpha,\beta} \bar{\nu}_R^{\alpha} H L_n^{\beta} + h.c.$$

where α and β are flavor index. For non-diagonal flavour Hamiltonian $H^{\alpha,\beta}$ and/or non-diagonal flavour Yukawa coupling $Y_1^{\alpha,\beta}$, $Y_2^{\alpha,\beta}$, this Lagrangian will produce mixing among three neutrino flavours. Here we are considering the case of diagonal flavour matrices hence no mixing is produced.

Hierarchy	n	ϵ	t	Yukawa Couplings
Normal	8	15	0.5	$\{Y^{1,1}, Y^{2,2}, Y^{3,3}\} = \{0.1, 0.31, 0.7\}$
Inverted	8	15	0.5	$\{Y^{1,1}, Y^{2,2}, Y^{3,3}\} = \{0.7, 0.706, 0.1\}$

TABLE VIII: BP points for the model with $Y_1 = Y_2 = \text{diag}\{Y^{1,1}, Y^{2,2}, Y^{3,3}\}$ producing neutrino mass in agreement with experimental data.

V. PHENOMENOLOGICAL SIGNATURES

The coupling introduced between BSM fields and SM fields to explain the neutrino mass production will have contributions to SM processes and hence can be phenomenologically tested.

$$\mathcal{L}_{int} = -Y \tilde{H} \bar{L}_L R_{n+1} + h.c. \quad (36)$$

After changing the basis to the mass eigenvectors χ_k of the matrix M_{CW} , the Lagrangian interaction term can be rewritten as [16]

$$\mathcal{L}_{\text{int}} = -Y \bar{L}_L \tilde{H} \mathcal{U}_{n+1,k} \chi_k \equiv - \sum_{k=1}^{n+1} Y_k \bar{L}_L \tilde{H} \chi_k \quad (37)$$

One of the biggest observable signatures this extra vertex introduces is the charged lepton flavour violation branching ratio. In SM, the contribution to $BR(\mu \rightarrow e\gamma)$ comes via higher-order loops and hence is very tiny $O(10^{-55})$ but these new vertices in the Lagrangian lead to drastic increment to this value of BR and hence puts one of the most stringent bound and also is one of the best channels to discover new physics. These new BSM fields can directly manifest themselves in collider experiments as the missing energies or displaced vertex as in LPL depending on their decay widths. These BSM neutrinos will also affect the cross-section of various processes at LEP and Hadron colliders via new Feynman diagrams as explained in the below section. Since, the gears-SM interaction term 37 couples Higgs with these SM-BSM fields, this leads to gears contributing to Higgs self-energy and also to possible Higgs decay width depending on the masses of new fields as discussed below. The other possible phenomenological signatures are discussed in [40].

A. Branching Ratio of FCNC

1. For Clockwork Variant Models

The Feynman diagram contributing to FCNC $BR(\mu \rightarrow e\gamma)$ is shown in Fig. 15. Since these models introduce extra heavy neutral leptons as the propagator in this diagram, the BR will deviate significantly from the SM FCNC BR. In the clockwork models, the $\mu \rightarrow e\gamma$ branching ratio is [41],[42]

$$\text{Br}(\mu \rightarrow e\gamma) = \frac{3\alpha}{8\pi} |\mathcal{A}|^2, \quad (38)$$

$$\mathcal{A} = \sum_{\alpha=1}^3 \sum_{j=1}^{N+1} V_{\mu\alpha} V_{e\alpha}^* \left| (U_{L\alpha})^{0j} \right|^2 F \left(\frac{m_{j,\alpha}^2}{m_W^2} \right), \quad (39)$$

with

$$F(x) = \frac{1}{6(1-x)^4} (10 - 43x + 78x^2 - 49x^3 + 4x^4 + 18x^3 \log x)$$

Fig.19 compares BR obtained for Lepton flavour violation in the $\mu \rightarrow e\gamma$ process with various CW scenarios. For bigger values of hopping strengths, the BR decreases for all CW variants and most of

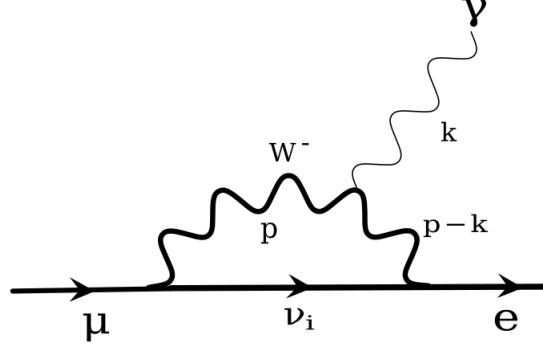


FIG. 15: Feynman diagram depicting the lepton flavour change channel.

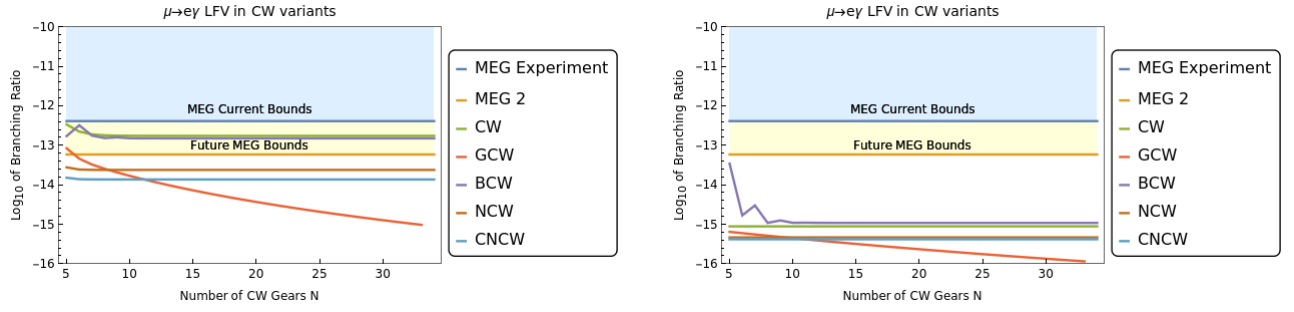


FIG. 16: For these plots, the scenario considered is $p=0.01$, $q=-1.7$ with $q'=q/2.5$ for BCW (left) and $q=-5$ with $q'=q/3$ for BCW (right) and $q^i=q$ for NCW and CNCW and $q_i = q - 0.1 \times i$ for GCW. The number of CW gears considered is on the x-axis.

these variants stabilise after a certain value of the number of CW gears considered. Hence energy scale at the order of 10 TeV with this set of parameters will survive the experimental constraints put up by the MEG experiment $BR(\mu \rightarrow e\gamma) \leq 4.2 \times 10^{-13}$ [31] and are within reach of upcoming experiments for some parameter space with sensitivity up to 6×10^{-14} [32].

2. For Fine-Cancellation Model

Similar to the clockwork model, in this model the FCNC branching ratio for $\mu \rightarrow e\gamma$ is given by the above equations (38), (39) since the mixing in the considered scenario is not produced by the model. In the case of mixing being also produced by this model, the BR expression would have been given by a similar expression [43]. The elements considered for the mixing matrix were experimental PMNS values with unitarity conditions to good significant digits. The variation of BR for the benchmark

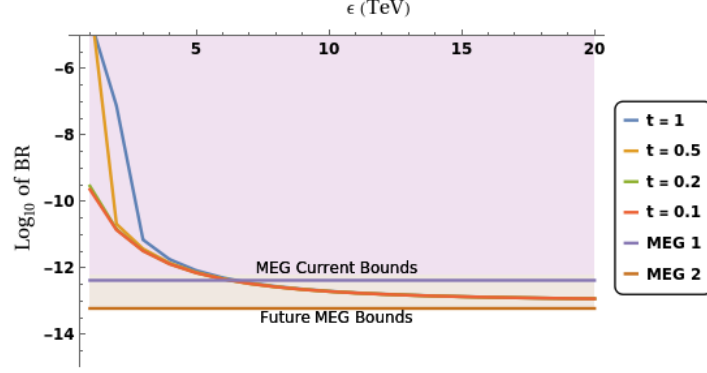


FIG. 17: This plot shows the log of BR with base 10 vs model scale parameter ϵ with $n = 8$ BP and various hopping couplings in the fine-cancellation model.

point (BP) with varying numbers of sites is shown in the below figure Fig 17: As can be seen from the plot, the BP survives the current MEG bounds but they are within the reach of future MEG constraints. The pink region denotes the ruled-out parameter space region.

B. Collider Signatures

The new BSM heavy neutral leptons will have impact on collider physics and their effects can be observed at a high enough energy collider as is elaborated in [28]. These new contributions are emerging from the weak sector. These extra contributions in weak currents from the massive BSM neutrinos will affect the cross sections observed at colliders. The SM charged current Lagrangian is

$$\mathcal{L}_{CC} = \frac{g}{a} W_{\mu}^{-} J_W^{\mu+} + \text{h.c.},$$

where g is the SM weak coupling, and

$$J_W^{\mu+} = \frac{1}{\sqrt{2}} \bar{e}_{\alpha} \gamma^{\mu} \nu_{L\alpha} \quad (40)$$

$$= \sum_{j=1}^{n+1} \frac{(U_{L\alpha})^j}{\sqrt{2}} \bar{e}_{\alpha} \gamma^{\mu} P_L \nu_{j,\alpha}. \quad (41)$$

with

$$\nu_{L\alpha} = \sum_{j=1}^{n+1} (U_{L\alpha})^j P_L \nu_{j,\alpha}$$

Here α represents flavour index, and $P_L = \frac{1-\gamma_5}{2}$ is the left-handed projection operator and $(U_{L\alpha})^j$ is the component of α flavour neutrino on j^{th} massive neutral lepton. Similarly, the neutral current will also

have contributions from these massive neutrinos. In [28] authors have studied the effects of neutrinos in both these CC and NC channels at hadron ($pp \rightarrow 3l + \cancel{E}_T$) and lepton colliders ($e^+e^- \rightarrow l\nu jj$) for various CW neutrinos masses and have given the signal-background distributions. The variants of CW models studied in this paper will have similar results as the fundamental mechanism is the same in all variants. The deviations will occur due to slight differences in the masses spectrum and coupling strengths produced in each variant.

C. Higgs Decay Width & Radiative Corrections

The nonzero coupling of BSM particles such as clockwork fermions with SM Higgs field will inevitably lead to corrections in Higgs mass. The leading order corrections occur at the 1-loop level. Consider the uniform CW model

$$\mathcal{L}_{CW} = \mathcal{L}_{kin} - \sum_i^{n-1} m \bar{L}_i R_i - \sum_i^{n-1} m q \bar{L}_i R_{i+1} + h.c. \quad (42)$$

with SM interaction part of Lagrangian in CW basis as

$$\mathcal{L}_{int} = -Y \tilde{H} \bar{L}_L R_n + h.c. \quad (43)$$

This term is written in CW mass basis once the link fields achieve vev as (37). Alternatively one can use the basis $N_L = (\nu_L, N_{L1}, N_{L2}, \dots, N_{Ln})$ and $N_R = (N_{R0}, N_{R1}, N_{R2}, \dots, N_{Rn})$ with transformations

$$N_{Rk} = \frac{1}{\sqrt{2}} (\chi_k + \chi_{k+n}), \quad k = 0, \dots, n$$

$$N_{Lk} = \frac{1}{\sqrt{2}} (-\chi_k + \chi_{k+n}), \quad k = 1, \dots, n.$$

to write it as [16]

$$\mathcal{L}_{int} = - \sum_{k=0}^n Y_k \bar{L}_L \tilde{H} N_{Rk} + h.c. \quad (44)$$

Once the Higgs achieves a vev and breaks the SM symmetry, the physical basis once again rotates. Using SVD the rotation of left $N_L = U N'_L$ and right basis $N_R = V N'_R$ is determined. The terms giving mass to N_L and N_R after Higgs achieves vev are

$$\begin{aligned} \mathcal{L}_{mass} &= -\bar{N}_L m_\nu^D N_R - \frac{v}{\sqrt{2}} \sum_{k=0}^n Y_k \bar{\nu}_L N_{Rk} + h.c. \\ &= -\bar{N}_L m_\nu^D N_R - \bar{N}_L M_{int} N_R \end{aligned} \quad (45)$$



FIG. 18: These Feynman diagrams show the 1-loop contribution of fermions in Higgs mass radiative corrections. The Left diagram shows it for the same fermions in the loop with y_{ii} coupling and the right diagram shows it for different fermions in the loop with y_{ij} coupling strength.

m_ν^D has the form of diagonal matrix and M_{int} matrix has only one non-zero row in these basis. Using the fact that diagonalization of the matrix $m_\nu^D + M_{int}$ with U and V unitary matrices does not guarantee the diagonalization of the individual matrix m_ν^D and M_{int} by these same unitary matrices, we find that SM Higgs gets mass corrections also from the fermionic-loops in which running fermions are not the same. The interaction of Higgs with new fields is covered by the following lagrangian :

$$\begin{aligned}
 \mathcal{L}_h &= -\frac{h}{\sqrt{2}} \sum_{k=0}^n Y_k \bar{\nu}_L N_{Rk} + h.c. \\
 &= -\frac{h}{v} \bar{N}_L M_{int} N_R + h.c. \\
 &= -\frac{h}{v} \bar{N}'_L U^\dagger M_{int} V N'_R + h.c.
 \end{aligned} \tag{46}$$

since $U^\dagger M_{int} V \neq M_D$ is not necessarily a diagonal matrix, if the coupling between the Higgs field and different fermions is strong enough it will have some implications on the Higgs hierarchy problem. The following Feynman diagrams give the radiative corrections to Higgs mass at the 1-loop level: The amplitude for 1-loop with the same fermions in the loop, $m_i = m_j = m$ and $y_{ij} = y_{ii}$ is given by

$$\Pi_R(q, \mu) = N_f \frac{12y_{ii}^2}{(4\pi)^2} \left(\frac{q^2}{18} - \frac{m^2}{3} + \int_0^1 dx \Delta^2 \ln \left(\frac{\Delta^2}{\mu^2} \right) \right) \tag{47}$$

N_f is the number of flavours. The contribution to Higgs's mass is proportional to coupling \times mass of fermions.

$$\delta m_h^2 \propto (y_{ii}^2)(m^2) \tag{48}$$

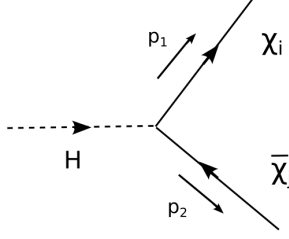


FIG. 19: Feynman Diagram for Higgs decay.

Hence, it slightly worsens the Higgs boson mass hierarchy similar to other TeV scale BSM models. A similar result is obtained for different fermions in the loop. Calculation for this case is done in the appendix.

Finally, consider the impact on Higgs decay width. Consider Higgs decaying to two particles χ_i and χ_j of masses m_1 and m_2 and four-momenta p_1 and p_2 with M mass of Higgs and q four-momentum. $H(q) \rightarrow \chi_i(p_1) + \chi_j(p_2)$. The Feynman diagram for the decay is given by 19: The decay rate for this process is:

$$\Gamma = \frac{4\pi}{4M} \frac{|\bar{M}|^2}{(2\pi)^2} \frac{\sqrt{E_1^2 - m_1^2}}{2M}$$

with

$$|\bar{M}|^2 = 2y_{ij}^2 (M^2 - (m_1 + m_2)^2)$$

Now for $m_1 + m_2 > M$, the decay width will not be positive real hence no decay contribution will be there if the sum of mass of BSM fields is bigger than Higgs boson mass. One can easily tweak the parameters of the described models to get gear of masses heavier than Higgs mass while surviving the BR, and collider constraints and also satisfying the experimentally observed value for neutrino mass. So, Higgs width will not achieve any new gear contributions and no further constraints from Higgs invisible decay width data will be imposed for gear field masses $> 125\text{GeV}$.

VI. CONCLUSION

In this paper, firstly the variants of well-known clockwork suppression models have been explored. It is shown that the underlying mechanism for variants of clockwork is the same for all cases. We

found that for some parameter ranges, the variants of clockwork will require a lesser number of sites to produce the same scale as the ordinary clockwork. The analytical expression for 0-mode in some cases of variants of clockwork is found to contain a combinatorial factor which for $0.5 < |q| < 2$ gives significantly enhanced localization and produces smaller scale than ordinary clockwork and for $|q| > 2$ differed from a few factors to few orders of magnitude from the clockwork depending on the numbers of gears considered. Also, the non-local clockwork models relax the constraint of $|q| > 1$ to get localization, in these models the localization of 0-mode can be achieved even with coupling terms being equal to mass terms. The smallest mass scale produced by CW for $q = 1$ with $n = 40$ is $O(10^{-3})$ of the fundamental parameter scale whereas with the same number of sites and with $q = q' = 1$ NNN-CW produced scale $O(10^{-11})$. As the number of sites increase, the NNN-CW will produce bigger and bigger suppresses scale compared to CW since the combinatorial factor will increase. Then, we have mentioned the fine cancellation mechanism to produce hierarchically small scales from natural order fundamental parameters in dimensional deconstruction perspective. This mechanism has been applied to SM to account for small neutrino mass problems. It can also be extended to account for PMNS mixing of SM active neutrinos along with their masses. The cancellation mechanism is applied in this paper for a specific case of local underlying theory space though one can consider other non-local theory spaces as well.

Finally, phenomenology for all these models was studied using the observable FCNC BR of $\mu \rightarrow e\gamma$ process and some comments were made about BSM effects in colliders and Higgs width/mass. We have laid out some benchmark points which satisfactorily produce neutrino mass as per the current experimental observations of mass squared difference and are also surviving current MEG experiment bounds. These Benchmark Points are within the reach of future MEG experiments and hence will be tested soon. All the BSM Lagrangians discussed in this paper can be straightforwardly extended to Majorana neutrino cases.

VII. ACKNOWLEDGEMENTS

The author would like to express his sincere gratitude to Prof. Sudhir Vempati for the insightful discussions and guidance throughout the research process. The author would also like to thank G. Kurup for the clarification of their work in the same direction. AS thanks CSIR, Govt. of India for SRF fellowship No. 09/0079(15487)/2022-EMR-I. The author also acknowledges the open-source software tools and community resources that were invaluable in the data analysis and visualization

aspects of this work, including Mathematica, Python, and the various scientific computing libraries. The code used by the author for data generation in this paper will soon be made available on GitHub for open access under a Creative Commons (CC) license to allow researchers to freely access, use, and build upon the codes, promoting transparency and reproducibility of the research presented in this paper.

-
- [1] Peter Minkowski. $\mu \rightarrow e\gamma$ at a rate of one out of 109 muon decays? *Physics Letters B*, 67(4):421–428, 1977.
 - [2] Tsutomu Yanagida. Horizontal gauge symmetry and masses of neutrinos. *Conf. Proc. C*, 7902131:95–99, 1979.
 - [3] M Gell-Mann, P Ramond, and R Slansky. Supergravity ed p van nieuwenhuizen and dz freedman. *Amsterdam: North-Holland* p, 315:79–18, 1979.
 - [4] SL Glashow. The future of elementary particle physics. In *Quarks and Leptons: Cargèse 1979*, pages 687–713. Springer, 1980.
 - [5] Rabindra N Mohapatra and Goran Senjanović. Neutrino mass and spontaneous parity nonconservation. *Physical Review Letters*, 44(14):912, 1980.
 - [6] J. Schechter and José W. F. Valle. Neutrino masses in $su(2) \otimes u(1)$ theories. *Physical Review D*, 22(9):2227, 1980.
 - [7] André De Gouvêa. Neutrino mass models. *Annual Review of Nuclear and Particle Science*, 66:197–217, 2016.
 - [8] Sacha Davidson, Enrico Nardi, and Yosef Nir. Leptogenesis. *Phys. Rept.*, 466:105–177, 2008.
 - [9] Nima Arkani-Hamed, Savas Dimopoulos, Gia Dvali, and John March-Russell. Neutrino masses from large extra dimensions. *Physical Review D*, 65(2):024032, 2001.
 - [10] Nima Arkani-Hamed, Andrew G Cohen, and Howard Georgi. Electroweak symmetry breaking from dimensional deconstruction. *Physics Letters B*, 513(1-2):232–240, 2001.
 - [11] Christopher T Hill, Stefan Pokorski, and Jing Wang. Gauge invariant effective lagrangian for kaluza-klein modes. *Physical Review D*, 64(10):105005, 2001.
 - [12] Tomas Hällgren, Tommy Ohlsson, and Gerhart Seidl. Neutrino oscillations in deconstructed dimensions. *Journal of High Energy Physics*, 2005(02):049, 2005.
 - [13] Lisa Randall and Raman Sundrum. An alternative to compactification. *Physical Review Letters*, 83(23):4690, 1999.
 - [14] Lisa Randall and Raman Sundrum. Large mass hierarchy from a small extra dimension. *Physical review letters*, 83(17):3370, 1999.

- [15] Gian F Giudice and Matthew McCullough. A clockwork theory. *Journal of High Energy Physics*, 2017(2):1–39, 2017.
- [16] Alejandro Ibarra, Ashwani Kushwaha, and Sudhir K Vempati. Clockwork for neutrino masses and lepton flavor violation. *Physics Letters B*, 780:86–92, 2018.
- [17] Thomas Hambye, Daniele Teresi, and Michel HG Tytgat. A clockwork wimp. *Journal of High Energy Physics*, 2017(7):1–19, 2017.
- [18] Seong Chan Park and Chang Sub Shin. Clockwork seesaw mechanisms. *Physics Letters B*, 776:222–226, 2018.
- [19] Avik Banerjee, Subhajit Ghosh, and Tirtha Sankar Ray. Clockworked VEVs and Neutrino Mass. *JHEP*, 11:075, 2018.
- [20] Teruyuki Kitabayashi. Clockwork origin of neutrino mixings. *Phys. Rev. D*, 100(3):035019, 2019.
- [21] Aqeel Ahmed and Barry M Dillon. Clockwork goldstone bosons. *Physical Review D*, 96(11):115031, 2017.
- [22] Daniele Teresi. Clockwork dark matter. *arXiv preprint arXiv:1705.09698*, 2017.
- [23] Kieran Wood, Paul M Saffin, and Anastasios Avgoustidis. Clockwork cosmology. *Journal of Cosmology and Astroparticle Physics*, 2023(07):062, 2023.
- [24] Miguel G Folgado, Andrea Donini, and Nuria Rius. Gravity-mediated dark matter in clockwork/linear dilaton extra-dimensions. *Journal of High Energy Physics*, 2020(4):1–46, 2020.
- [25] Florian Niedermann, Antonio Padilla, and Paul M Saffin. Higher order clockwork gravity. *Physical Review D*, 98(10):104014, 2018.
- [26] Cheng-Wei Chiang and Bo-Qiang Lu. Testing clockwork axion with gravitational waves. *Journal of Cosmology and Astroparticle Physics*, 2021(05):049, 2021.
- [27] David E. Kaplan and Riccardo Rattazzi. Large field excursions and approximate discrete symmetries from a clockwork axion. *Phys. Rev. D*, 93(8):085007, 2016.
- [28] Sungwoo Hong, Gowri Kurup, and Maxim Perelstein. Clockwork neutrinos. *Journal of High Energy Physics*, 2019(10):1–30, 2019.
- [29] Ido Ben-Dayan. Generalized clockwork theory. *Physical Review D*, 99(9):096006, 2019.
- [30] Nathaniel Craig and Dave Sutherland. Exponential hierarchies from anderson localization in theory space. *Physical Review Letters*, 120(22):221802, 2018.
- [31] Y Bao, F Berg, J Egger, M Hildebrandt, Z Hodge, PR Kettle, A Mtchedilishvili, A Papa, F Renga, S Ritt, et al. Search for the lepton flavour violating decay $\mu^+ \rightarrow e^+ \gamma$ with the full dataset of the meg experiment: Meg collaboration. *The European Physical Journal C-Particles and Fields*, 76(8):434–434, 2016.
- [32] Alessandro M. Baldini et al. The Search for $\mu^+ \rightarrow e^+ \gamma$ with 10–14 Sensitivity: The Upgrade of the MEG Experiment. *Symmetry*, 13(9):1591, 2021.
- [33] P. A. Zyla et al. Review of Particle Physics. *PTEP*, 2020(8):083C01, 2020.
- [34] I. Esteban et al. Nufit4.1 at nufit webpage, <http://www.nu-fit.org>. Accessed: 2023-07-10.

- [35] Adam Tropper and JiJi Fan. Randomness-assisted exponential hierarchies. *Physical Review D*, 103(1):015001, 2021.
- [36] Nima Arkani-Hamed, Andrew G Cohen, and Howard Georgi. (de) constructing dimensions. *Physical Review Letters*, 86(21):4757, 2001.
- [37] Kenneth Lane. Deconstructing dimensional deconstruction. *Nuclear Physics B-Proceedings Supplements*, 117:731–734, 2003.
- [38] Tomas Hällgren. *Phenomenological studies of dimensional deconstruction*. PhD thesis, KTH, 2005.
- [39] Philip W Anderson. Absence of diffusion in certain random lattices. *Physical review*, 109(5):1492, 1958.
- [40] Gian F Giudice, Yevgeny Kats, Matthew McCullough, Riccardo Torre, and Alfredo Urbano. Clock-work/linear dilaton: structure and phenomenology. *Journal of High Energy Physics*, 2018(6):1–70, 2018.
- [41] TP Cheng and Ling-Fong Li. $\mu \rightarrow e \gamma$ in theories with dirac and majorana neutrino-mass terms. *Physical Review Letters*, 45(24):1908, 1980.
- [42] Ernest Ma and A Pramudita. Exact formula for $(\mu \rightarrow e \gamma)$ -type processes in the standard model. *Physical Review D*, 24(5):1410, 1981.
- [43] Ta-Pei Cheng and Ling-Fong Li. *Gauge theory of elementary particle physics*. Oxford university press, 1994.

Appendix A: Linear Algebra Results

Theorem : Let M be an $m \times n$ matrix and N be an $n \times k$ matrix then $\text{rank}(MN) \leq \text{rank}(M)$.

Hence matrix of the form $A^\dagger A$ will always have a non-zero dimensional kernel space.

Proof : Consider N as matrix A and use the fact that the rank of an $m \times n$ matrix M is the dimension of the range $R(M)$ of the matrix M with the range given by

$$R(M) = \{y \in \mathbb{R}^m \mid y = Mx \text{ for some } x \in \mathbb{R}^n\}$$

Consider the rotated left and right basis to be χ_L and χ_R respectively i.e,

$$L = \mathcal{U}\chi_L, \quad R = \mathcal{V}\chi_R$$

It's easy to show that for a symmetric matrix, the SVD gives identical left and right modes rotation. For a real symmetric positive definite matrix M ,

$$\begin{aligned}
M^\dagger &= M, \\
MM^\dagger &= M^\dagger M \\
\mathcal{U}^\dagger MM^\dagger \mathcal{U} &= \mathcal{M}_{diag} \\
\mathcal{U}^\dagger M^\dagger M \mathcal{U} &= \mathcal{M}_{diag} \\
\mathcal{V}^\dagger M^\dagger M \mathcal{V} &= \mathcal{M}_{diag}
\end{aligned} \tag{A1}$$

hence, $\mathcal{U} = \mathcal{V}$ though \mathcal{U} and \mathcal{V} are unique only when the original matrix is positive definite.

Appendix B: One Loop Calculations

The amplitude for 1-loop with fermions of different masses is given by

$$i\Pi_{1L} = -N_f (-iy_{ij})^2 \text{Tr} \left[\int \frac{d^4 k}{(2\pi)^4} \frac{i(\not{k} + m_i)}{[k^2 - m_i^2]} \frac{i(\not{k} + \not{q} + m_j)}{[(k+q)^2 - m_j^2]} \right] \tag{B1}$$

N_f is the number of flavours. In the limit when both fermions in the loop are the same, $m_i = m_j = m$ and $y_{ij} = y_{ii}$. Using dimensional regularization, we get the familiar result

$$\Pi(q^2) = N_f \frac{12y_{ii}^2}{(4\pi)^2} \mu^{2\epsilon} \int_0^1 dx \Delta^2 \left(\frac{1}{\hat{\epsilon}} + \ln \left(\frac{\Delta^2}{\mu^2} \right) - \frac{1}{3} \right)$$

where,

$$\int_0^1 dx \Delta^2 = \int_0^1 dx (-q^2 x(1-x) + m^2) = m^2 - \frac{q^2}{6}$$

Thus, we can write the following expression for the amplitude:

$$\Pi(q^2) = N_f \frac{12y_{ii}^2}{(4\pi)^2} \mu^{2\epsilon} \left[\frac{1}{\hat{\epsilon}} \left(m^2 - \frac{q^2}{6} \right) + \frac{q^2}{18} - \frac{m^2}{3} + \int_0^1 dx \Delta^2 \ln \left(\frac{\Delta^2}{\mu^2} \right) \right]$$

Using the \overline{MS} scheme we obtain the radiative mass correction to Higgs as:

$$\Pi_R(q, \mu) = N_f \frac{12y_{ii}^2}{(4\pi)^2} \left(\frac{q^2}{18} - \frac{m^2}{3} + \int_0^1 dx \Delta^2 \ln \left(\frac{\Delta^2}{\mu^2} \right) \right) \tag{B2}$$

Now, consider the scenario with two different fermions coupled to Higgs, $m_i \neq m_j$ and coupling with Higgs is y_{ij} . The amplitude is

$$\begin{aligned} i\Pi_{1L} &= -N_f(-iy_{ij})^2 \text{Tr} \left[\int \frac{d^4k}{(2\pi)^4} \frac{i(\not{k} + m_i)}{[k^2 - m_i^2]} \frac{i(\not{k} + \not{q} + m_j)}{[(k+q)^2 - m_j^2]} \right] \\ &= -N_f i^4 y_{ij}^2 \int \frac{d^4k}{(2\pi)^4} \text{Tr} \left[\frac{(\not{k} + m_i)}{[k^2 - m_i^2]} \frac{(\not{k} + \not{q} + m_j)}{[(k+q)^2 - m_j^2]} \right] \end{aligned} \quad (\text{B3})$$

using,

$$\text{Tr}\{(\not{k} + m_i)(\not{k} + \not{q} + m_j)\} = 4(k \cdot q + k^2 + m_i m_j)$$

plugging this in (B3) and using Feynman parametrization of the propagators i.e.,

$$\frac{1}{AB} = \int_0^1 dx \frac{1}{[Ax + B(1-x)]^2}$$

Taking $A = (k+q)^2 - m_j^2$ and $B = k^2 - m_i^2$ we get:

$$\begin{aligned} Ax + B(1-x) &= x[(k+q)^2 - m_j^2] + (k^2 - m_i^2)(1-x) \\ &= (k^2 + q^2 + 2qk - m_j^2)x + k^2 - m_i^2 - k^2x + m_i^2x \\ &= k^2 - m_i^2 + q^2x + 2qkx - m_j^2x + m_i^2x \pm q^2x^2 \\ &= (k+qx)^2 + q^2x - q^2x^2 - m_j^2x + m_i^2x - m_i^2 \\ &= (k+qx)^2 + q^2x(1-x) - m_i^2 + x(m_i^2 - m_j^2) \\ &= (k+qx)^2 - \Delta'^2 \end{aligned} \quad (\text{B4})$$

with $\Delta'^2 = -(q^2x(1-x) - m_i^2 + x(m_i^2 - m_j^2))$, we see that in the limit $m_i = m_j$, $\Delta'^2 = \Delta^2$.

$$\frac{1}{(k^2 - m_i^2)[(k+q)^2 - m_j^2]} = \int_0^1 dx \frac{1}{[(k+qx)^2 - \Delta'^2]^2}$$

plugging this parametrization in (B3), We obtain the following amplitude expression:

$$i\Pi(q^2) = -4N_f y_{ij}^2 \int_0^1 dx \int \frac{d^4k}{(2\pi)^4} \frac{k^2 + m_i m_j + kq}{[(k+qx)^2 - \Delta'^2]^2}$$

After performing the variable shift $k \rightarrow k + qx \equiv l$, the numerator becomes:

$$\begin{aligned} k^2 + m_i m_j + kq &= (l - qx) \cdot q + (l - qx)^2 + m_i m_j \\ &= l \cdot q - q^2 x + l^2 + q^2 x^2 - 2l \cdot qx + m_i m_j \end{aligned} \quad (\text{B5})$$

eliminating all the linear terms in l^μ and redefining l as k , we obtain:

$$i\Pi(q^2) = -4N_f y_{ij}^2 \int_0^1 dx \int \frac{d^4 k}{(2\pi)^4} \frac{k^2 + m_i m_j - q^2 x(1-x)}{[k^2 - \Delta'^2]^2} \quad (\text{B6})$$

Next, we use Dimensional Regularization to compute the integrals of the following type

$$I_1 = \int \frac{d^d k}{(2\pi)^d} \frac{k^2}{(k^2 + \Delta')^2} = \frac{1}{(4\pi)^{\frac{d}{2}}} \frac{d}{2} \frac{\Gamma(2 - \frac{d}{2} - 1)}{\Gamma(2)} \left(\frac{1}{\Delta'}\right)^{2 - \frac{d}{2} - 1} \quad (\text{B7})$$

and

$$I_2 = \int \frac{d^d k}{(2\pi)^d} \frac{1}{(k^2 + \Delta')^2} = \frac{1}{(4\pi)^{\frac{d}{2}}} \frac{d}{2} \frac{\Gamma(2 - \frac{d}{2})}{\Gamma(2)} \left(\frac{1}{\Delta'}\right)^{2 - \frac{d}{2}} \quad (\text{B8})$$

using dim. reg. in (B6) about $d = 4 - \epsilon$, and expanding up to $O(\epsilon)$ we get:

$$\begin{aligned} \Pi(q^2) = & -4N_f y_{ij}^2 \int_0^1 dx \left[\frac{\Delta'^2}{4\pi^2 \epsilon} + \frac{\Delta'^2 (2\log(\mu^2) - 2\gamma_E + 1 + \log(16\pi^2) - 2\log(-\Delta'^2))}{16\pi^2} \right. \\ & \left. + (m_i m_j - q^2 x(1-x)) \left\{ \frac{1}{8\pi^2 \epsilon} - \frac{\gamma_E + \log(-\Delta'^2) - \log(4\pi) - \log(\mu^2)}{16\pi^2} \right\} \right] + O(\epsilon) \quad (\text{B9}) \end{aligned}$$

using the renormalization scheme and putting all the divergences in the counterterms, we get

$$\begin{aligned}
\Pi_R(q^2, \mu) &= -4N_f y_{ij}^2 \int_0^1 dx \left[\frac{\Delta'^2(1 - 2\log(\frac{-\Delta'^2}{\mu^2}))}{16\pi^2} + (m_i m_j - q^2 x(1-x)) \left\{ -\frac{\log(\frac{-\Delta'^2}{\mu^2})}{16\pi^2} \right\} \right] + O(\epsilon) \\
&= -\frac{4N_f y_{ij}^2}{16\pi^2} \left[\frac{m_i^2}{2} + \frac{1}{2}(m_j^2 - q^2) + \frac{q^2}{3} - \frac{1}{18q^4} \left\{ 6(m_i^4 - 2m_i^2(m_j^2 + q^2) + (m_j^2 - q^2)^2) \right\}^{3/2} \times \right. \\
&\quad \tanh^{-1} \left(\frac{m_i^2 - m_j^2 - q^2}{\sqrt{m_i^4 - 2m_i^2(m_j^2 + q^2) + (m_j^2 - q^2)^2}} \right) - 6(m_i^4 - 2m_i^2(m_j^2 + q^2) + (m_j^2 - q^2)^2)^{3/2} \\
&\quad \times \tanh^{-1} \left(\frac{m_i^2 - m_j^2 + q^2}{\sqrt{m_i^4 - 2m_i^2(m_j^2 + q^2) + (m_j^2 - q^2)^2}} \right) + 2q^2 \left(3m_i^4 - 3q^2(-3m_i^2 - 3m_j^2 + q^2) \right. \\
&\quad \times \log \left(-\frac{m_j^2}{\mu^2} \right) - 6m_i^2(m_j^2 + 2q^2) + 3m_j^4 - 12m_j^2 q^2 + 5q^4 \Big) - 3 \log(m_i^2) \left(m_i^6 - 3m_i^4(m_j^2 + q^2) \right. \\
&\quad \left. \left. + 3m_i^2(m_j^4 - q^4) - (m_j^2 - q^2)^3 \right) + 3 \log(m_j^2) \left(m_i^6 - 3m_i^4(m_j^2 + q^2) + 3m_i^2(m_j^4 - q^4) - \right. \right. \\
&\quad \left. \left. - 36m_i m_j q^2 - 6m_j^4 + 6m_j^2 q^2 + 5q^4 \right) - 6\sqrt{m_i^4 - 2m_i^2(m_j^2 + q^2) + (m_j^2 - q^2)^2} \left(2m_i^4 - m_i^2 \right. \right. \\
&\quad \left. \left. (4m_j^2 + q^2) + 6m_i m_j q^2 + 2m_j^4 - m_j^2 q^2 - q^4 \right) \tanh^{-1} \left(\frac{m_i^2 - m_j^2 - q^2}{\sqrt{m_i^4 - 2m_i^2(m_j^2 + q^2) + (m_j^2 - q^2)^2}} \right) \right. \\
&\quad \left. + 6(2m_i^4 - m_i^2(4m_j^2 + q^2) + 6m_i m_j q^2 + 2m_j^4 - m_j^2 q^2 - q^4) \sqrt{m_i^4 - 2m_i^2(m_j^2 + q^2) + (m_j^2 - q^2)^2} \right. \\
&\quad \left. \tanh^{-1} \left(\frac{m_i^2 - m_j^2 + q^2}{\sqrt{m_i^4 - 2m_i^2(m_j^2 + q^2) + (m_j^2 - q^2)^2}} \right) - 3 \log(m_j^2) \left(2m_i^6 - 3m_i^4(2m_j^2 + q^2) \right. \right. \\
&\quad \left. \left. + 6m_i^3 m_j q^2 + 6m_i^2 m_j^4 + m_i(6m_j q^4 - 6m_j^3 q^2) - 2m_j^6 + 3m_j^4 q^2 - q^6 \right) + 3 \log(m_i^2) \left(2m_i^6 - 3m_i^4 \right. \right. \\
&\quad \left. \left. (2m_j^2 + q^2) + 6m_i^3 m_j q^2 + 6m_i^2 m_j^4 + m_i(6m_j q^4 - 6m_j^3 q^2) - 2m_j^6 + 3m_j^4 q^2 - q^6 \right) \right\} \Big] \quad (B10)
\end{aligned}$$

the energy independent contribution to Higgs's mass is proportional to coupling \times mass of fermions.

$$\delta m_h^2 \propto (y_{ij}^2)(m_i^2 + m_j^2) \quad (B11)$$

Appendix C: Higgs Decay Width

The decay rate for this process is:

$$d\Gamma = \frac{1}{2M} \frac{d^3 \vec{p}_1}{(2\pi)^3 2E_1} \frac{d^3 \vec{p}_2}{(2\pi)^3 2E_2} (2\pi)^4 \delta^4(q - p_1 - p_2) |\bar{M}|^2,$$

with $|\bar{M}|^2$ as the invariant matrix element squared. Momentum conservation imposes $p_1 \cdot p_2 = (M^2 - m_1^2 - m_2^2)/2$ with $p_1^2 = m_1^2$ and $p_2^2 = m_2^2$. The corresponding amplitude M is given by:

$$M = -iy_{ij}\bar{u}(p_1)v(p_2)$$

leading to:

$$\begin{aligned} |\bar{M}|^2 &= y_{ij}^2 (\text{Tr}[\not{p}_1 \not{p}_2] - m_1 m_2 \text{Tr}[1]) \\ &= 4p_1 \cdot p_2 - 4m_1 m_2 \\ &= 2y_{ij}^2 (M^2 - (m_1 + m_2)^2). \end{aligned}$$

Since the amplitude square $|M|^2$ is momentum-independent it can be taken outside the integration. Using $d^3\vec{p}_2/2E_2 = d^4p_2\delta^+(p_2^2 - m_2^2)$ and carrying out the d^4p_2 integration it comes out

$$d\Gamma = \frac{1}{2M} \frac{|\bar{M}|^2}{(2\pi)^2} \int \frac{d^3\vec{p}_1}{2E_1} \delta^+((q - p_1)^2 - m_2^2).$$

In the rest frame of the Higgs boson, $q = (M, 0, 0, 0)$, hence the argument of the δ^+ function reduces to $(M^2 - 2ME_1 + m_1^2 - m_2^2)$. Now, integrating the expression over \vec{p}_1 to get the decay width as:

$$d\Gamma = \frac{1}{2M} \frac{|\bar{M}|^2}{(2\pi)^2} \int \frac{p_1^2 d\vec{p}_1 d\phi d\theta \sin\theta}{2E_1} \delta^+(M^2 - 2ME_1 + m_1^2 - m_2^2).$$

using the fact that $\vec{p}_1 d\vec{p}_1 = E_1 dE_1$,

$$d\Gamma = \frac{1}{4M} \frac{|\bar{M}|^2}{(2\pi)^2} \int \frac{\vec{p}_1 E_1 dE_1 d\phi d\theta \sin\theta}{E_1} \delta^+(M^2 - 2ME_1 + m_1^2 - m_2^2).$$

this integral is non-zero for the value of E_1 that will lead to the Dirac-Delta function with 0 as the argument i.e.,

$$\begin{aligned} M^2 - 2ME_1 + m_1^2 - m_2^2 &= 0 \\ E_1 &= \frac{M^2 + m_1^2 - m_2^2}{2M} \end{aligned} \tag{C1}$$

$$\Gamma = \frac{4\pi}{4M} \frac{|\bar{M}|^2}{(2\pi)^2} \frac{\sqrt{E_1^2 - m_1^2}}{2M}$$